Electric Power Systems Research 151 (2017) 68–85

Contents lists available at ScienceDirect

Electric Power Systems Research

journal homepage: www.elsevier.com/locate/epsr

Smart grid realization with introducing unified power quality conditioner integrated with DC microgrid

Pouria Goharshenasan Khorasani, Mahmood Joorabian*, Seyed Ghodratollah Seifossadat

Department of Electric Power Engineering, Engineering Faculty, Shahid Chamran University, Ahvaz, Iran

ARTICLE INFO

Article history:
Received 3 February 2017
Received in revised form 13 May 2017
Accepted 15 May 2017

Keywords:
Hybrid AC/DC microgrid
Power quality
Power swing
Power flow control
Smart grid
UPQC-DC

ABSTRACT

This paper presents a new design of the hybrid AC/DC microgrid for optimization of the performance of the smart grid. This design by using the capacity of the DC microgrid and introducing a new unified power quality conditioner, named UPQC-DC, and providing appropriate control schemes for two back to back interface converter between the AC and DC microgrids, presents important characteristics such as power quality improvement, power flow control, reactive power compensation, and elimination of power swings. The proposed method guarantees the realization of all aforementioned goals in both grid connected and isolated modes for the first time. Several computer simulations are performed using Matlab/Simulink software for verifying the proposed scheme.

1. Introduction

Nowadays, there is a global trend toward smart grids to improve electric power systems. Although different definitions and meanings have been presented for smart grids, there is general consensus on their characteristics. According to the EISA 2007 report, the main objectives of smart grids are as follows [1]:

- Reliability, security, energy storage source (ESS), and distributed generation (DG);
- Energy efficiency, sustainability, and renewable inputs;
- Information technology, communication platform, and full cyber-security;
- Intelligent load management and grid-connected electric vehicles;
- Minimizing the unnecessary obstacles to the achievement of the aforementioned objectives.

Having reviewed the earlier studies and literature on DC microgrids [2–4], it was demonstrated that, in the presence of DC microgrids, most of the goals of smart grids could be realized faster, often at a lower cost, and with greater efficiency. However, since the majority of the power grids are presently AC type, AC microgrids are still dominant and purely DC microgrids are not expected to emerge exclusively in power grids. On the other hand, given the increased consumption of energy provided by AC grids compared to what they have been designed for, and the other problems, such as congested and high loss lines and overloaded transformers, there's a growing need for developing the structure of these grids. In addition, given the aforementioned advantages of DC microgrids, the development of current AC distribution networks can be implemented using DC microgrids. Consequently, linking AC microgrids with DC microgrids and employing the profits of the both microgrids, has become interesting in recent studies [5–16]. The idea is to merge the AC and DC microgrids through a bidirectional AC/DC converter and establishing a hybrid AC/DC microgrid in which AC or DC type energy sources and loads can flexibly integrate into the microgrids and power can smoothly flow between the two microgrids indicating the realization of hybrid AC/DC microgrids [5]. On the other hand, the current electronic loads of consumers are mainly sensitive and require high power quality [17]. So, the idea of power conversion of DC microgrid through providing a new design for hybrid AC/DC microgrid can serve as an effective solution for the current problems of electricity networks. By doing so, the needs of loads are covered and the standards of power quality are realized and it can be seen as a step toward future smart grids. In this regard, one of the recent research projects that have received a great deal of attention in the optimization of the performance of smart grids is the hybrid AC/DC microgrids.

The work done in this area fits into the following subject categories: new control methods and schemes (e.g., centralized and decentralized control) of hybrid AC/DC microgrids [5–7], energy

* Corresponding author.
E-mail address: mjoorabian@scu.ac.ir (M. Joorabian).

http://dx.doi.org/10.1016/j.epsr.2017.05.023
0378-7796/

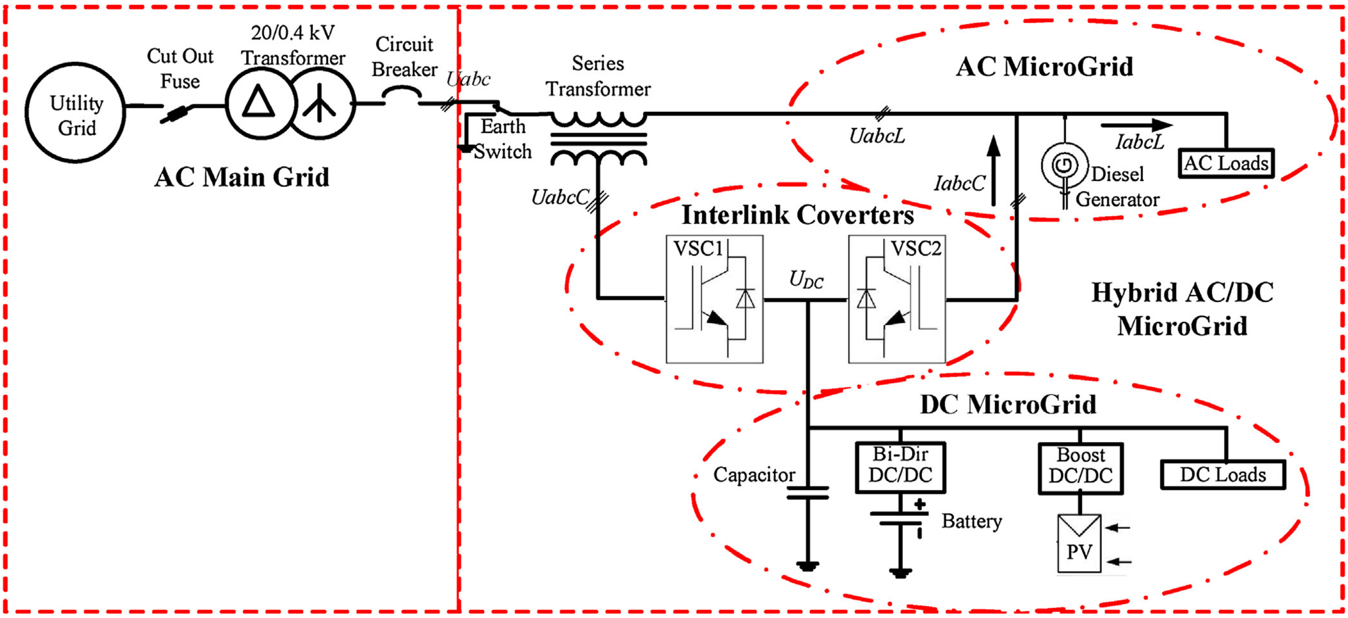

Fig. 1. The proposed structure of the hybrid AC/DC microgrid.

management strategies for renewable energy sources and energy storages in hybrid systems [8–10], new control schemes for power converters between AC and DC microgrids as well as interface converters of different microgrid sources [11–13], design of hybrid AC/DC microgrids with the aim of improving efficiency and power quality, reducing the energy wastes, control the voltage profile and network stability [14–16]. Having reviewed the studies conducted in this regard, an obvious research lack was found in detail studying the power quality issue on these microgrids. Although the issue of improving the power quality of AC microgrid employing active filters, dynamic voltage restorers (DVRs), unified power quality conditioners (UPQCs) and the interface converter between sources and microgrid, have been proposed in various articles [17–20]. However, given the structural differences of hybrid AC/DC microgrids, appropriate structures still need to be analyzed and proposed to use the maximum capacity and potential of these microgrids. To this end, firstly, a new scheme of UPQC family is presented in Section 2 for developing the AC grid into a hybrid AC/DC microgrid. Secondly, the proposed control schemes are explained in Section 3. Then, the simulated model and the results of the simulations of different scenarios are presented in Section 4, and finally, the conclusion is presented in Section 5.

2. The proposed structure of the hybrid AC/DC microgrid

The proposed structure for the hybrid AC/DC microgrid is shown in Fig. 1. The mentioned system originated from developing a conventional AC microgrid with a DC microgrid which is connected to the AC system by two back-to-back interlink converters. Each part of the proposed system is identified with a dash-dot circle in Fig. 1. The AC microgrid includes AC loads, synchronous generators and LV lines. The DC microgrid includes DC loads, batteries, capacitors, photovoltaic (PV) generators and DC/DC converters. The interlink converters are bi-directional type with IGBT switches.

The proposed hybrid AC/DC microgrid, corresponding to the unified power quality conditioners, is introduced as the 13th member of this family by the title of UPQC-DC. It is worth noting that the detailed review of the UPQCs types falling into 12 different families is presented in Ref. [21]. The UPQC-DG controller described in Ref. [20] has the strongest similarity to the proposed scheme with this difference that the proposed scheme is broadly responsible for controlling the hybrid microgrids, covering the voltage and frequency stability, controlling the two-way power flow between the AC and DC microgrids, and maintaining the power quality even in the isolated mode (even in the worst load quality). In the proposed scheme, although the DC microgrid provides the DC power of local loads, it serves as a collection line, receiving the DC power from renewable energy sources and exchanging power with different energy storages and AC microgrid. As for AC microgrid, although it provides the traditional AC loads, it absorbs the energy produced by synchronous generators and AC grid and exchange a part of the power with DC microgrid.

What follows is an overview of various features that can be realized through the multi-objective UPQC-DC controller design.

2.1. Improving the quality of the voltage and current

One of the main objectives of the present research is using the hybrid AC/DC microgrids to maintain the total harmonic distortion (THD) of the microgrid voltage and the total demand distortion (TDD) of the microgrid currents below 5% (according to the IEEE 519 standard [22]) and to keep the amplitude variations of the microgrid voltage in the range of ±5% (according to the IEEE 1159 standard [23]) under different power quality problems.

In Fig. 2a, a simple representation of the compensation of power quality in the grid connected mode is shown. As can be seen in the compensation representation, due to utilizing the DC microgrid capacity and the realization of two freedom degrees for each converter, the compensation diagrams has a four-quarter and circular coverage. In this state, any variation of the load currents (IabcL) can compensate with parallel compensator currents (IabcC), then the drawn currents from the AC grid (IabcS) can remain pure sinusoidal. Subsequently, any variation in the grid voltages (Uabc) can compensate with series compensator voltages (UabcC), then the delivered voltages to the AC microgrid (UabcL) can remain pure sinusoidal.

One of the innovations of the present research is the possibility of providing microgrid with standard voltage in the isolated mode while the load currents have the worst quality. It is worth noting that, in the typical hybrid microgrids [12–16] in the isolated mode,

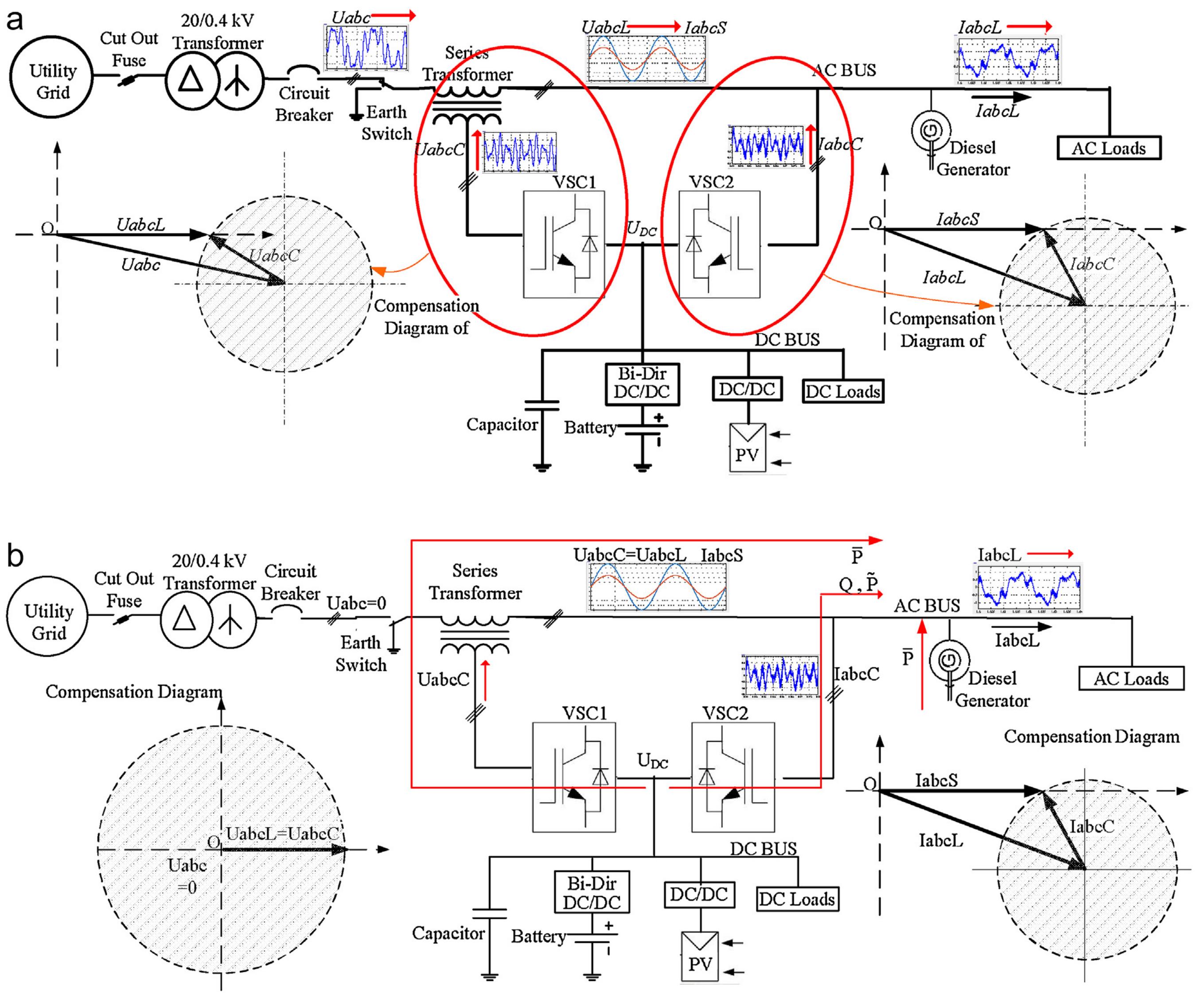

Fig. 2. (a) A simple representation of the compensation of power quality in the grid connected mode. (b) A simple representation of the compensation of power quality in the isolated mode.

the quality of the delivered voltage is proportional to the conditions of the consumer loads and allows for no guarantee of power quality. In Fig. 2b, a simple representation of the compensation of power quality in the isolated mode is shown. In the current scheme, an automatic earth switch provided a path to flow the zero sequence current after the microgrid was disconnected from the main grid. In this case, the first (series) and second (parallel) converters played the roles of a static synchronous voltage source (SSVS) and an active power filter (APF), respectively. In this state, SSVS can supply the isolated microgrid with pure sinusoidal voltage (UabcC), while APF compensated any variation of the load currents (IabcL).

2.2. Frequency stability and power swings compensation of AC microgrid

One of the major problems of AC microgrids is the frequency stability and the power swings in the isolated mode, about which numerous studies have been conducted [24–27]. However, another innovation of the present research was explaining how the proposed scheme could compensate all fluctuations attributable to the islanding/connecting process or the entry/exit of the loads/sources or any fault in the microgrids through using an extra frequency control loop on the control system of the series converter.

2.3. The compensation of the reactive power of loads

Another advantage of the proposed scheme is the continuous compensation of the reactive power resulting from the non-linear or induction loads of consumers. This conduce to maintain the power factor close to one for all sources of AC microgrid in both grid connected and isolated modes. In this case, a great portion of the capacity of distribution transformers and AC sources feeding the AC microgrid is released. On the other hand, in addition to reduced power distribution losses, the need for common reactive compensators is minimized in sub-transmission substations. The paths of power flow and the manner of reactive power compensation are shown in Fig. 3.

2.4. Power conversion between AC and DC microgrids

In the proposed hybrid microgrid scheme, controlling the production of various distributed generation units is based on the decentralized droop control method [6], whereas a coordinated

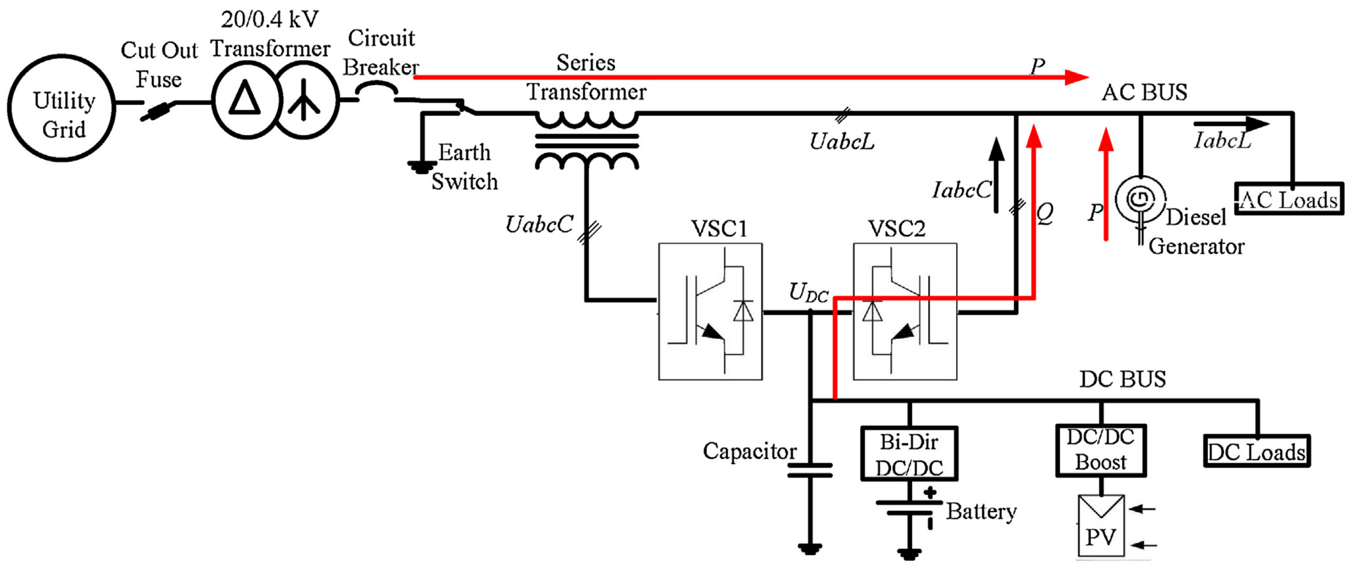

Fig. 3. The paths of power flow and the manner of reactive power compensation.

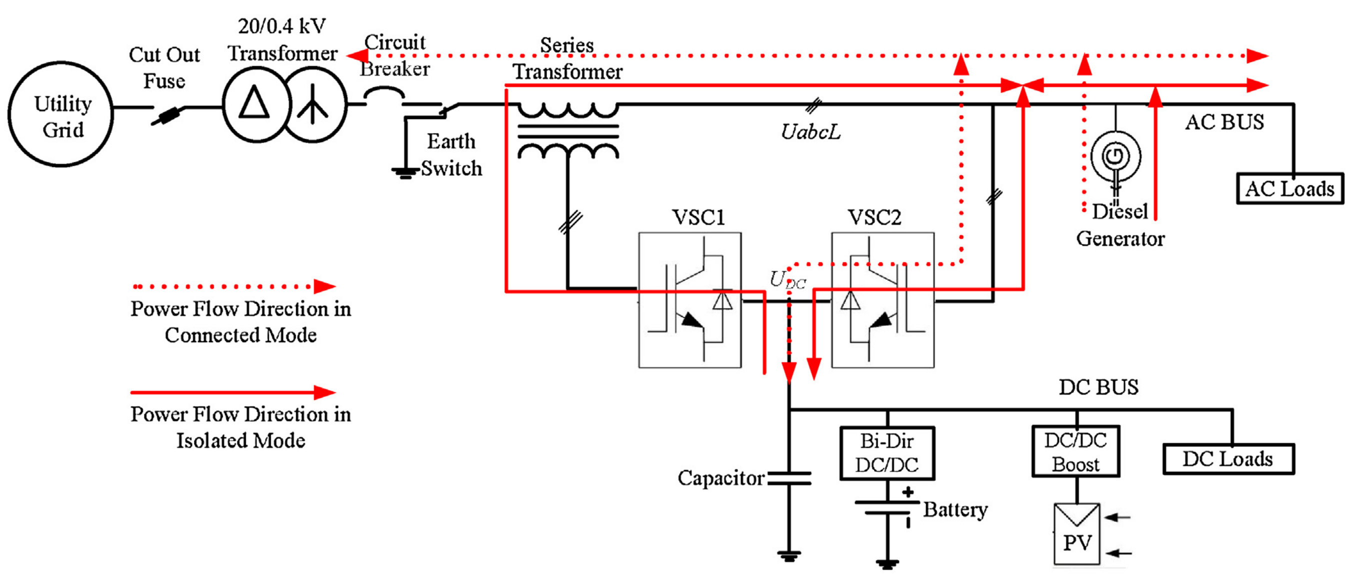

Fig. 4. The possible paths of power flow in the proposed hybrid microgrid.

AC/DC control method is suggested for proper power flow between the two microgrids. The principle of the proposed method is based on simultaneously capturing and analyzing the data relating to the frequency changes of AC microgrid as well as the voltage changes of DC microgrid [5,11]. The coordinated AC/DC control system, particularly manage the power conversion between AC and DC microgrids. In Fig. 4, an overview of the all possible paths of power flow is shown in the proposed hybrid microgrid.

3. The design of the proposed control systems for the hybrid AC/DC microgrid

To achieve the objectives outlined in the previous section using the potential of the hybrid AC/DC microgrid, the proposed control schemes are presented for each of the power converters of the UPQC-DC controller.

3.1. The control scheme of the parallel converter of the UPQC-DC

The control structure shown in Fig. 5 is suggested for generating the current reference signal of the parallel converter of the hybrid microgrid. The mentioned control system is designed in such a way that in addition to removing all of the power quality problems relating to the load current [28] as well as compensating for the reactive power under various conditions, the power conversion is managed between the two microgrids, and the level of the voltage of the DC microgrid is adjusted at the level of U_{DCref}.

In Fig. 5, the parameters of *UabcL*, *IabcL*, *IabcC*, *Pset*, U_{DC} and ωt represent the values of the three phase voltage of load, three phase current of load, three phase reference signal for parallel compensator, the set point value of the power conversion, the voltage of the DC microgrid and angular position of the voltage phasor of *UabcL*, respectively. The function of the proposed control system is so that the active and reactive components of the load current (*Ip* & *Iq*) are first extracted based on the pq theory [29] at any moment

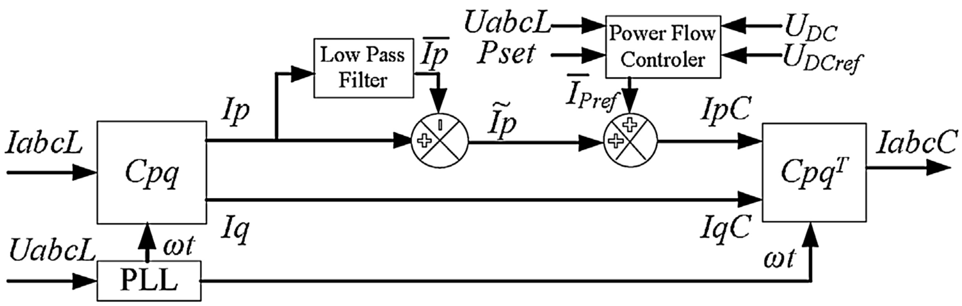

Fig. 5. The proposed control system for the parallel converter of the hybrid microgrid.

along with applying *Cpq* conversion and the phase lock on the load voltage. The *Cpq* conversion is shown in (1).

$$Cpq=\sqrt{\frac{2}{3}}\begin{bmatrix}\mathrm{Sin}(\omega t) & \mathrm{Sin}(\omega t-\frac{2\pi}{3}) & \mathrm{Sin}(\omega t+\frac{2\pi}{3})\\ -\mathrm{Cos}(\omega t) & -\mathrm{Cos}(\omega t-\frac{2\pi}{3}) & -\mathrm{Cos}(\omega t+\frac{2\pi}{3})\end{bmatrix}$$

$$Ipq = Cpq \times IabcL, \; IabcC = Cpq^{T} \times IpqC \quad (1)$$

According to the instantaneous power theory [29], each of the active and reactive components of the load current possesses a moderate value ($^{-}$) and a fluctuating value ($^{\sim}$) (including all of the disturbances of the power quality). According to this theory, each of these values can be selected and compensated with the aim of compensation.

In the present article, since the parallel compensation involves the compensating of any harmonic distortion and reactive components of load currents, so all reactive components (I_q) and the fluctuating part of the active component ($\tilde{I_P}$) of the load current should be provided by the compensator.

So, as shown in Fig. 5, the average values of the active components ($\overline{I_P}$) are calculated by the low pass filter, which is then subtracted from the total value (I_p), and the result would be the fluctuating value ($\tilde{I_P}$). Further, the power flow controller (the coordinated AC/DC control system) provides the necessary control signal ($\overline{I}_{pref}$) for exchanging the required power between the two AC and DC microgrids based on the proposed model in Fig. 6. Finally, by applying the transpose conversion of *Cpq* transform (Cpq^T) [29], on the calculated active and reactive currents (*IpqC*), the three-phase reference currents or the currents which should be compensated (*IabcC*) are extracted as (1). Due to some reasons, including high response speed, simplicity of the structure and lower cost [19], the hysteresis method is employed for implementing the proposed control scheme.

3.1.1. The coordinated AC/DC control system

Unlike the standalone AC or DC microgrid, power conversion in the hybrid AC/DC systems is unattainable through the conventional droop methods because during the isolated operation, the interface convertor simultaneously plays the role of a feeder for a microgrid and the role of a consumer for another microgrid [9]. Therefore, a new control method is required for controlling the power flow. In this paper, a hybrid droop method is presented for controlling the power conversion in the interface converter of the AC/DC microgrid, whereby the value of the active power required for transferring from one network to another is determined through the simultaneous measurement of the frequency of the AC microgrid and the voltage of the DC microgrid as well as using the hybrid droop control shown in Fig. 6.

Assuming the exclusion of switching losses (*Pac* = *Pdc*), the relations governing the proposed control system in Fig. 6 are as presented in Eqs. (2)–(11).

$$\mathrm{P_{DCref}} = \frac{1}{\mathrm{K_{DC}}}(\mathrm{U_{DCref}} - U_{\mathrm{DCo}}) \quad (2)$$

$$\mathrm{K_{DC}} = \frac{1}{\mathrm{P_{DCmax}}}(\mathrm{U_{DCmax}} - U_{\mathrm{DCmin}}) \quad (3)$$

$$\mathrm{U_{DCo}} = \sqrt{\mathrm{U_{DCref}}\ 2 - \frac{1}{\mathrm{K}_{\omega o}}(\Delta\omega)} \quad (4)$$

$$\Delta\omega = 2\pi f - \omega \quad (5)$$

$$\mathrm{K}_{\omega o} = \mathrm{K}_{\omega}(\frac{1}{2}\frac{\mathrm{C_{dc}}}{\mathrm{Ts}}) \quad (6)$$

$$\mathrm{K}_{\omega} = D + (\frac{1}{\mathrm{R_1}} + \frac{1}{\mathrm{R_2}} + \ldots + \frac{1}{\mathrm{R_n}}) \quad (7)$$

$$P_{ACref} = \frac{1}{K_{AC}}(\Delta\omega o) \quad (8)$$

$$\Delta\omega o = \mathrm{K}_{\omega o}(U_{\mathrm{DCref}}\ 2 - U_{\mathrm{DC}}\ 2) \quad (9)$$

$$\mathrm{K_{AC}} = \frac{1}{\mathrm{P_{ACmax}}}(\omega_{\max} - \omega_{\min}) \quad (10)$$

$$\mathrm{P_{ref}} = P_{\mathrm{set}} + P_{\mathrm{DCref}} + P_{\mathrm{ACref}} \quad (11)$$

where:

ω = The angular frequency of the AC microgrid
$\Delta\omega$ = The angular frequency deviation from the reference value
$K_{\omega o}$ = The slope of the AC–DC droop characteristic
K_{DC} = The slope of the DC droop characteristic
K_{AC} = The slope of the AC droop characteristic
P_{set} = Power sharing set point
P_{DCref} = The exchange rate of power from the DC microgrid to AC
P_{ACref} = The exchange rate of power from the AC microgrid to DC
P_{ref} = The reference signal of power exchange between the two microgrids
U_{DCo} = The calculated voltage of the DC link
$U_{DC\max}$ = The maximum allowable voltage of the DC link
$U_{DC\min}$ = The minimum allowable voltage of the DC link
$P_{DC\max}$ = The maximum power of the DC link
$P_{AC\max}$ = The maximum power of the AC source
K_{ω} = The slope of the droop characteristic of the AC microgrid
R_n = The droop coefficient of the *n*th synchronous generator
D = The load damping constant of the AC microgrid
C_{dc} = The capacitance of the DC microgrid
Ts = The sampling time of simulation
$\Delta\omega o$ = The calculated frequency changes of the AC microgrid
$\omega_{\max}$ = The maximum allowable frequency of the AC microgrid
$\omega_{\min}$ = The minimum allowable frequency of the AC microgrid

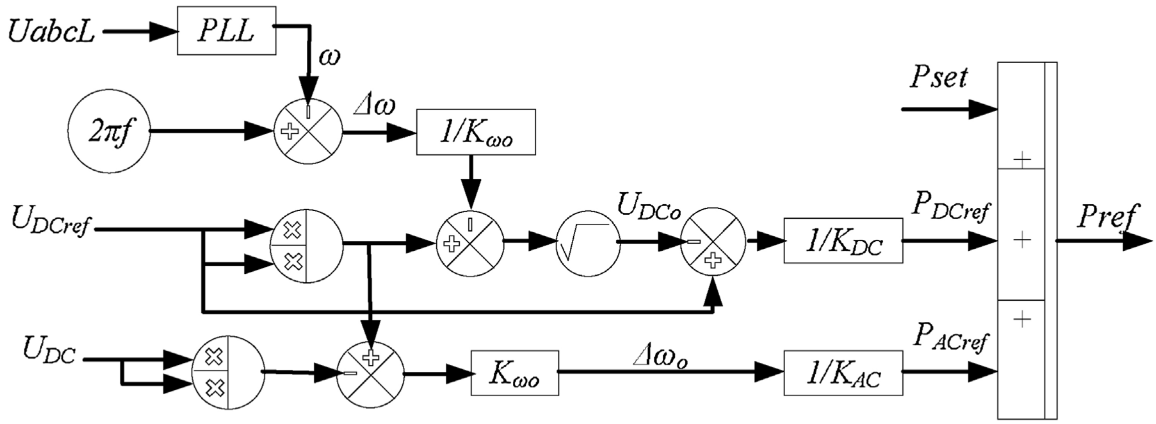

Fig. 6. The proposed model for the coordinated control of power exchange between the two AC/DC microgrids.

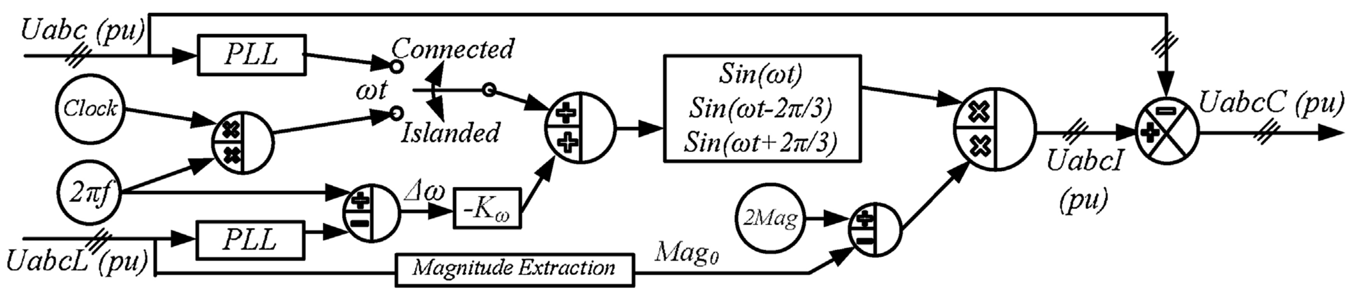

Fig. 7. The proposed control scheme for the series convertor of hybrid microgrid.
Where:
Uabc = The three-phase voltage of the main AC grid
ωt = The angular position of the *Uabc* voltage phasors in the grid connected mode, or the reference angular position in the isolated mode.
Mag = The set magnitude of the AC microgrid voltage
Mag_0 = The measured magnitude of the load voltage
UabcC = The reference voltage of the series compensator
UabcI = The ideal voltage to deliver to load

3.2. The control scheme of the series converter of the UPQC-DC

Given the specific tasks of the series controller, including the removal of all power quality problems associated with the grid voltage [28] (interruption, sag, swell, and voltage unbalance) and any change in the pure sinusoid form of the voltage wave form, removing the power swings, keeping synchronism, controlling the stability of the AC microgrid, developing an uninterrupted sinusoid power supply, and controlling the voltage of the microgrid; the control scheme presented in Fig. 7 is proposed.

The proposed control system presented in Fig. 7 functions in each of the grid connected and isolated modes as follows:

In the grid connected mode, the angular position of the AC grid voltage (ωt) is extracted through the phase lock on voltage zero crossing at any moment and is then added to the negative value of the fluctuations of the AC microgrid ($-K_\omega{}^*\ \Delta\omega$), and the resulting value is used as the sinusoid functions argument. Then, the ideal three-phase voltages are calculated through adjusting the *Mag* value to a desirable magnitude and comparing with the load voltage magnitude (See Eq. (12)). The amount of the voltage that should be injected into the grid by the compensator is calculated through comparing the ideal obtained voltages and the instantaneous voltages of the grid as Eq. (13).

$$UabcI = (2\mathrm{Mag} - \mathrm{Mag}_0)\cdot\begin{bmatrix}\mathrm{Sin}(\omega t - K_\omega{}^*\Delta\omega)\\ \mathrm{Sin}(\omega t - K_\omega{}^*\Delta\omega - 2\pi/3)\\ \mathrm{Sin}(\omega t - K_\omega{}^*\Delta\omega + 2\pi/3)\end{bmatrix} \tag{12}$$

$$UabcC = UabcI - Uabc \tag{13}$$

In the isolated mode, the angular position of the reference voltage of the AC microgrid is extracted through multiplying the ideal angular velocity of $2\pi f$ by the real time at any moment and is then added to the negative value of the fluctuations of the AC microgrid ($-K_\omega{}^*\ \Delta\omega$), and the resulting value is used as the sinusoid functions argument. Then, the ideal three-phase voltages are calculated through adjusting the *Mag* value to a desirable magnitude (usually one pu) and comparing with the load voltage magnitude. Given the opening of the main circuit breaker of the microgrid in the isolated mode, the value of the *Uabc* is zero. As a result, the ideal obtained voltage is the same amount of voltage that should be injected into the grid by the compensator (See Eq. (14)). More about power swing damping will be found in appendix.

$$UabcC = UabcI = (2\mathrm{Mag} - \mathrm{Mag}_0)\cdot\begin{bmatrix}\mathrm{Sin}(2\pi ft - K_\omega * \Delta\omega)\\ \mathrm{Sin}(2\pi ft - K_\omega{}^*\Delta\omega - 2\pi/3)\\ \mathrm{Sin}(2\pi ft - K_\omega{}^*\Delta\omega + 2\pi/3)\end{bmatrix} \tag{14}$$

Due to some reasons, including the popularity and simplicity of the structure and low cost for, the sinusoid pulse width modulation (SPWM) method is utilized to implement the proposed control scheme of the series converter [19].

4. The simulation of the hybrid AC/DC microgrid

To verify the validation of the proposed design of the UPQC-DC model and to examine the accuracy of the function of the proposed

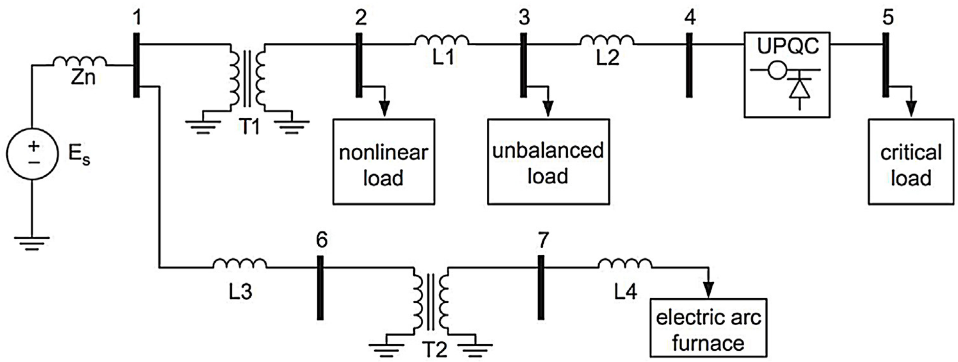

Fig. 8. The selected case study to verify the performance of the proposed UPQC-DC.

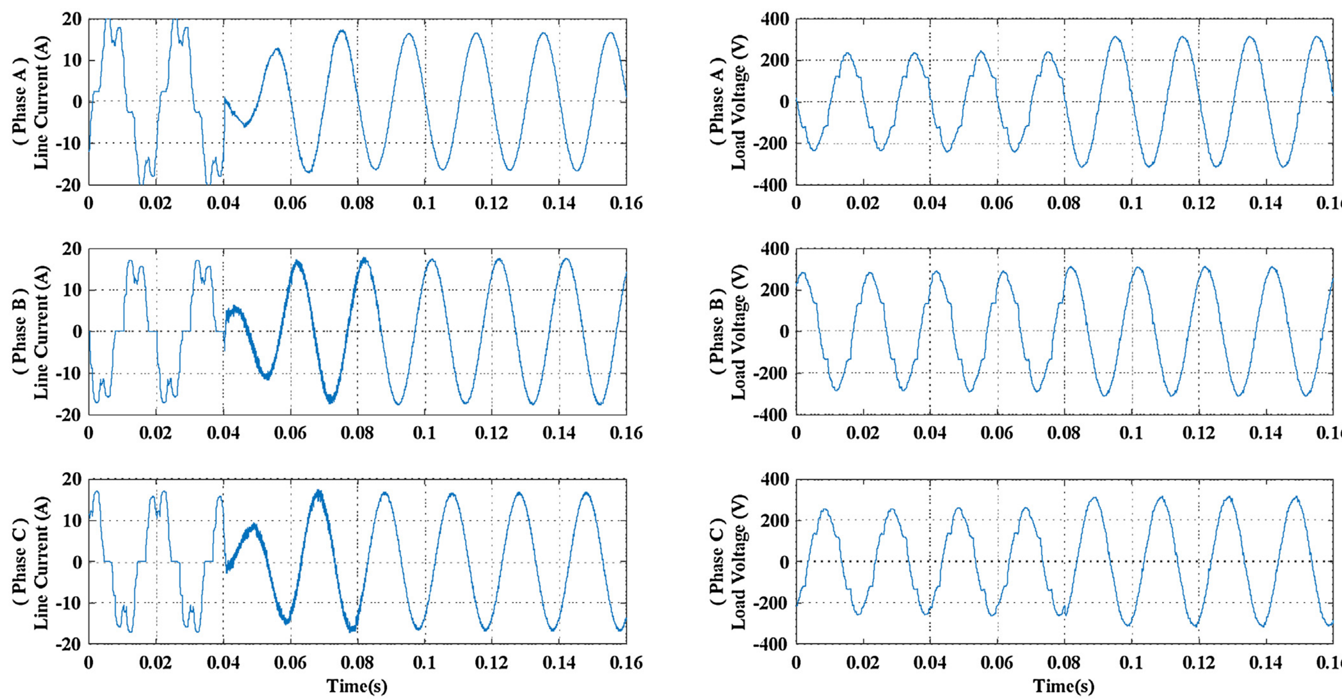

Fig. 9. The UPQC-DC compensation performance in damping of harmonics and voltage restoration.

scheme within the scope of the objectives listed in Section 2, several simulation is run and the results are presented in this section.

4.1. Verification of the proposed UPQC-DC model

According to the multi-function design of the proposed UPQC-DC model, at the first step, it should be able to perform the routine functions of the UPQC. Hence as regards to well describe example of UPQC compensation in Ref. [28], it selected as a case study. To verify the performance of the proposed UPQC-DC in the presence of several current and voltage disturbance sources, the model distribution system of Fig. 8 consisting of seven (linear and nonlinear) buses is considered. System specifications are listed in Table A1 in Appendix A. The load at bus 5 is a three-phase nonlinear load that is considered to be the critical load to be protected by the UPQC. This load consists of three power electronic converters. In this example harmonic distortion and voltage imbalance are imposed on the network (Application Example 9.13 in Ref. [28]). Shunt and series branches of the UPQC start to operate at t = 0.04 s and t = 0.08 s, respectively. Fig. 9 show the UPQC-DC performance in damping of harmonics in load voltage of bus 5 and line current of branch 2. Although the harmonic components of critical load are compensated by the shunt converter, the line current includes a high-frequency component before the operation of series branch occurs. After the operation of the series converter has occurred at t = 0.08 s, high-frequency components of currents are damped significantly as well as load voltage compensation. By comparison of the simulation results in Fig. 9 with those reported in Ref. [28], an excellent agreement is obtained demonstrating the accuracy of the proposed simulation.

4.2. Performance of the proposed UPQC-DC

To examine the accuracy of the function of the proposed scheme within the scope of the objectives listed in Section 2, the hybrid microgrid shown in Fig. 1 is simulated in detail using the Matlab/Simulink Software (see Fig. 10). The main AC grid is simulated through a programmable three phase voltage source, a circuit breaker, series impedance introducing distribution line, a set of cut-out fuses, three phase 20/0.4 kV transformer with nominal power capacity of 1 MVA and Dyn11 connection, a fault simulator, and a low voltage circuit breaker. The programmable three

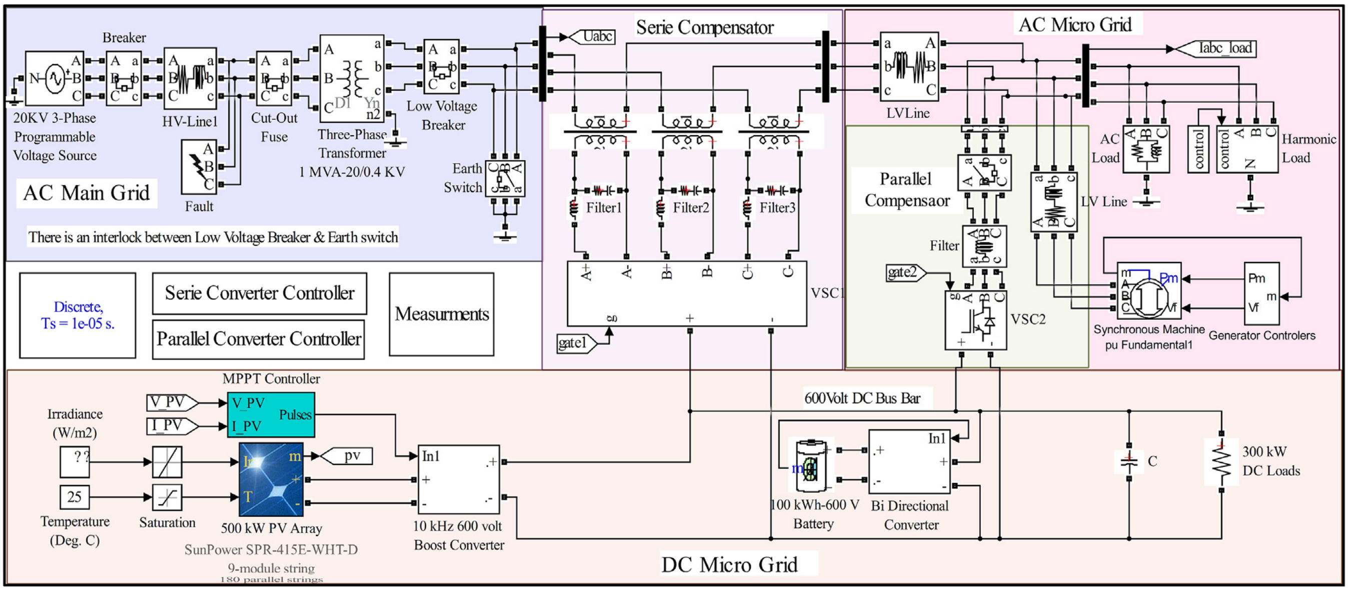

Fig. 10. The simulated model of proposed hybrid AC/DC microgrid in Matlab/Simulink.

phase voltage source, make it possible to implement a variety of harmonics, amplitude or phase imbalances and to represent different sequences (positive, negative and zero) in voltage wave forms of main feeder. The breakers make it possible to isolate the microgrid during any abnormal condition. The fault block provides the possibility of implementation of one-phase, two-phase or three-phase faults, with or without grounding, using different values of arc and ground resistances. Moreover, the AC microgrid comprised a distributed generation unit equipped with a synchronous generator, distribution lines, and active, reactive and harmonic loads. Here, assumed that, all of the loads are located at the end of the distribution line. The DC microgrid comprised a controlled photovoltaic (PV) generation unit through the maximum power point tracking, battery energy storage, capacitor and DC loads. In the proposed design, the main sources of the energy for DC microgrid are PV arrays that provided maximum productive energy of the cells into the DC network using a boost DC/DC converter. The interlink converters include of two series and parallel compensators. The series compensator comprised three single-phase converters which are connected to the grid through three series transformers and low pass filters. The switching is controlled through the pulse width modulation and natural sampling with 6 kHz modulation frequency. On the other hand, the parallel compensator comprised a three-phase converter which is connected to the load side grid through three inductive series filters. The three-phase converter is controlled through the Hysteresis method and the fixed sampling frequency of 10 kHz. Finally, the earth switch, interlocked with the low voltage circuit breaker, is opened and closed in the grid connected and isolated modes, respectively. It is worth noting, all of the parameters of the intended grid are mentioned in Table A2 in Appendix A. Further on, the results of different scenarios examined in the proposed model are mentioned in this section.

4.2.1. *First scenario*

Assumptions

- Connection state: grid connected mode.
- Active and reactive loads of AC microgrid: 800 kW and 400 kVar respectively.
- Harmonic contents of AC loads: 150 A of second harmonic, 500 A of fifth harmonic and 200 A of seventh harmonic.
- Harmonic contents of AC grid voltage: 55% of the 5th harmonic and 40% of the 7th harmonic.
- Steady state voltage drop of AC lines: 7%.
- Voltage sag due to the high impedance fault: 33% from 1.5 s until 1.6 s of simulation time.
- Total loads of DC microgrid: 300 kW.
- Available capacity of PV generation: 360 kW.

Given the above-mentioned assumptions, the wave forms of currents drawn from AC sources, the voltage delivered to the AC load, and the related harmonic spectrums before and after compensation are all shown in Fig. 11. Fig. 11a–f depicts the currents and voltages of AC microgrid before compensation, and the related wave forms after compensation are displayed in Fig. 11g–L. As can be seen, the current drawn from the AC grid contains 54.63% of the total harmonic distortions before compensation, and a power swing with a frequency of 2.5 Hz is evident (see Fig. 11a and b). However, after compensation, the current drawn from the grid is purely sinusoidal with 2.2% of the total harmonic distortions, and no power swings are observed after the fault occurrence (see Fig. 11g and h). More importantly, the currents drawn from the synchronous generator become definitely unstable in the event of prolonged fault establishment and exit the grid (see Fig. 11c). In this case, the harmonic distortions of the current drawn from the generator is limited to 23.8% because of the higher impedance of the generator (see Fig. 11d). However, despite the presented compensation plan, in addition to maintaining the stability of the synchronous generator and removing the power swings after the fault, the total harmonic distortions of the current drawn from the generator is restricted to 2.5% (see Fig. 11i and j). Finally, the status of the voltage delivered to the load is depicted in Fig. 11e under different power quality issues (presence of harmonics, drops and sags). Additionally, as can be seen in the harmonic spectrum in Fig. 11f, the total harmonic distortion of the grid voltage measured roughly 70%, and in this case, the grid conditions would not certainly remain stable. Further, in addition to the collapse of the synchronization of the AC generators due to the emergence of large negative components, the loads of consumers would undergo serious damages. However, given the proposed plan, the voltage delivered to the microgrid is purely sinusoidal with 2.5% of the total harmonic distortions as well as an amplitude of one pu (see Fig. 11k and L) (it is worth noting

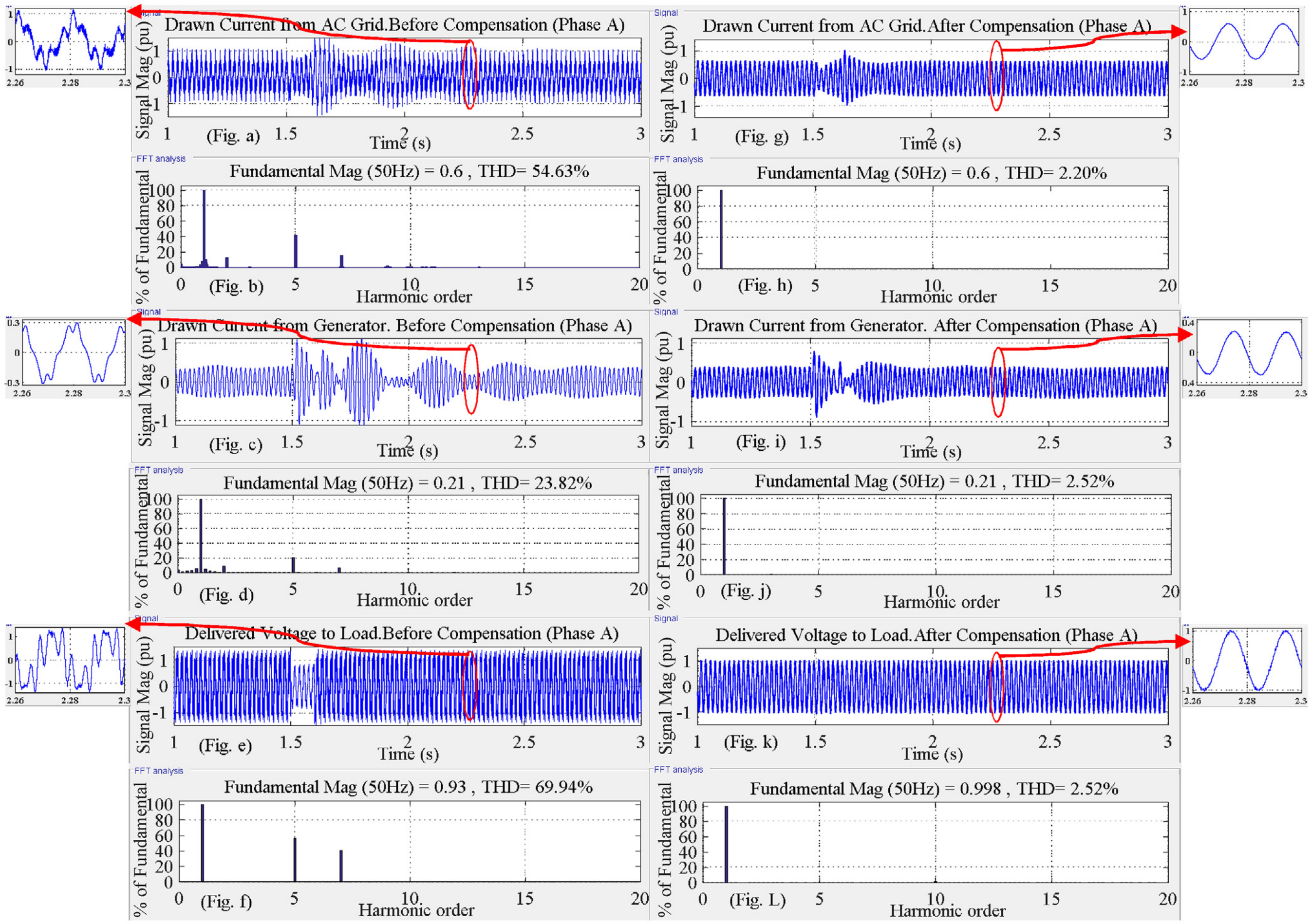

Fig. 11. Drawn currents from AC sources, delivered voltage to load, and related harmonic spectrums before & after compensation.

that all fast fourier transforms (FFTs) are applied during 2.5–3.0 s of simulation time).

The general status of the power flow, voltage control and adjusting the power factor of the AC sources in the AC/DC microgrid are described in Fig. 12. Fig. 12a shows the load current of the DC microgrid almost constant at 0.5 pu, or 500 A (300 kW), and as can be seen, the load current of the DC microgrid is least affected by the fault in the AC grid. Fig. 12b displays the load current of the AC microgrid almost constant at 0.9 pu, or 900 A, including both active and reactive components. In addition, in spite of the fault in the upstream grid, the load current received the minimal effects from the fault. Fig. 12c shows the current inflows to the DC microgrid through both series and parallel exchange links. As can be seen, upon the occurrence of the fault, the current of the series link rises to 0.2 pu in the negative direction (from the DC to AC microgrid) to cover the drop in the AC grid voltage, while the current of the parallel link in the positive direction (from the AC to DC microgrid) increases to cover the voltage drop in the DC microgrid. Fig. 12d displays the current of the PV boost converter in which around 0.6 pu (600 A) of the current is delivered to the DC microgrid at a rated voltage under maximum power point tracking (MPPT) method, and in the event of fault occurrence and reduced voltage, the output current is raised accordingly. The current of the microgrid batteries and their state of charge (SoC) are displayed in Fig. 12e and f, respectively. Additionally, as can be seen, until the occurrence of any faults in the AC microgrid, the excess of the production capacity of the solar cells charges the batteries with a current measuring roughly 0.07 pu (70 A). But as soon as the fault occurs, the battery SoC changes into the discharge mode and provides the required current of the series link to control the voltage of the AC microgrid. In Fig. 12g, the voltage of the DC microgrid is shown at one pu (600 V), and as can be seen, with the fault occurrence in the AC microgrid, the parallel converter (see Fig. 12c) injects the current deficit of the microgrid into the DC link and the voltage reduction of the DC microgrid is limited. Fig. 12h shows the voltage of the AC microgrid at one pu, and upon the fault and voltage sag occurrence as much as 33%, only a 2% voltage drop is imposed on the AC microgrid. In Fig. 12i, the current drawn from the AC grid is displayed. Under normal conditions, an active current of 0.6 pu (600 kW) is received from the grid, whereby 75% of the 800-kW load power is supplied. Upon the fault occurrence, the current drawn from the AC grid lessens (see Fig. 12i), and the deficit is compensated through raising the current of the generator (see Fig. 12j) in such a way that the load currents do not experience any deficits (see Fig. 12b). However, after fault clearance, the problem of power swings arises due to the surplus of energy in the microgrid, rupturing the balance between the generation and consumption. Given the control plan of the series converter, the energy balance is established in the microgrid by means of injecting a current proportional to the oscillations of the generator current, and the oscillations is damped in the very first cycle. Fig. 12j shows the current drawn from the AC generator (measuring approximately 0.2 pu (200 kW) under normal conditions), whereby the remaining 25% of the 800-kW load power is supplied. The explanation of how the generator functions at the time of fault occurrence was mentioned above. In Figs. 12k and L, the power factor of the AC grid and generator are shown,

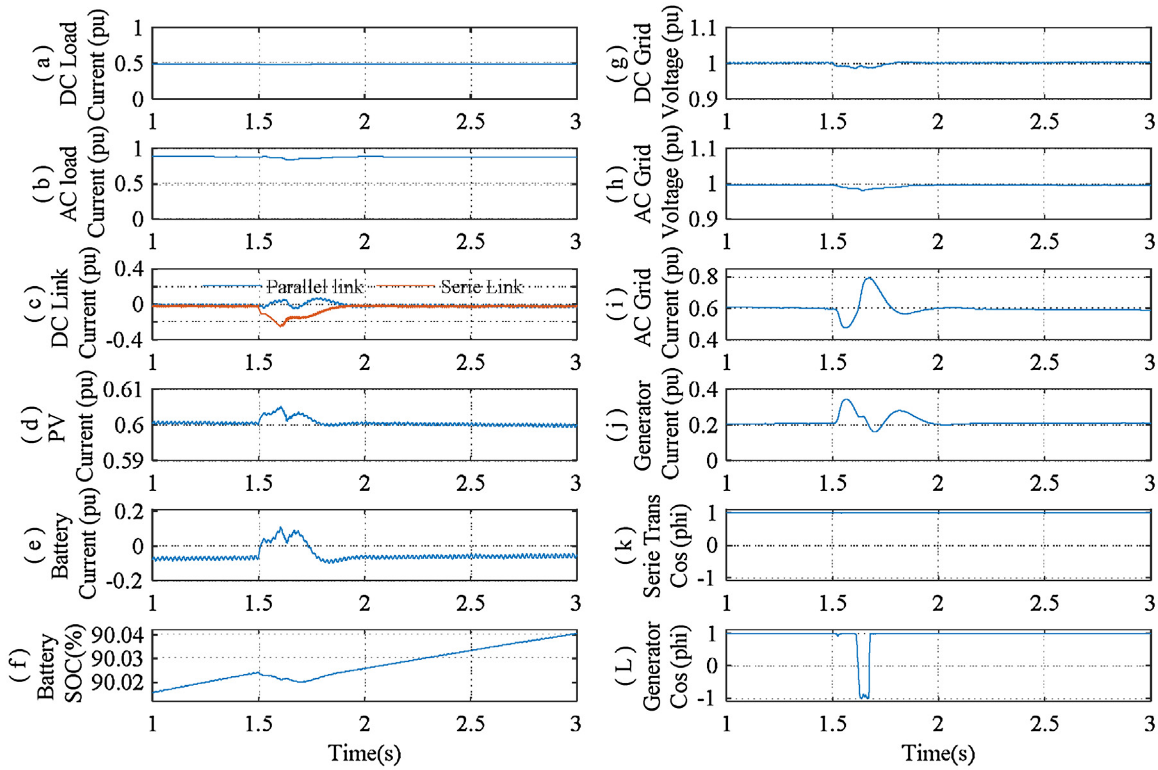

Fig. 12. The overall status of the power flow, voltage control and adjusting the power factor of the AC sources in hybrid microgrid.

respectively. Also, as can be seen, the parallel controller adjusts the power factor of the microgrid sources in a unit value. Furthermore, the direction of the generator current is reversed only at the time of fault clearance because of the power swing, and the power factor becomes −1.

4.2.2. Scenario two

Assumptions

- Connection state: grid connected mode.
- Active and reactive loads of AC microgrid: 800 kW and 400 kVar respectively.
- Harmonic contents of AC loads: 150 A of second harmonic, 500 A of fifth harmonic and 200 A of seventh harmonic.
- Harmonic contents of AC grid voltage: 55% of the 5th harmonic and 40% of the 7th harmonic.
- Steady state voltage drop of AC lines: 7%.
- Available capacity of PV generation: 360 kW.
- Total loads of DC microgrid: 300 kW which step up to 600 kW during 1.3–1.9 s.
- Energy conversion set point (Pset): change to 0.2 pu during 2.3–3 s.

Given the above-mentioned assumptions, Fig. 13 displays the overall status of the power flow, voltage control, and power factor correction in the hybrid AC/DC microgrid during the current scenario. In the first part of this scenario, a step up in the load of the DC microgrid from 300 kW to 600 kW results in a rise in the load current from 0.5 to about 0.95 pu (due to the drop of the voltage of the DC microgrid to 0.97 pu) (see Fig. 13a). This increase in the load current of the DC microgrid should be covered by the microgrid sources, but due to the limited available capacity (0.6 pu) of the PV unit (see Fig. 13e), the deficit of the load current is compensated through discharging the batteries of the microgrid to nearly 0.2 pu (see Fig. 13f) as well as a simultaneous rise in the current of the parallel DC link to around 0.2 pu (see Fig. 13c). Since the excess of the current of the parallel DC link is provided by the AC grid, the current drawn from the AC grid is raised proportional to the DC link current (see Fig. 13k). During the overload occurrence in the DC microgrid, the voltage and the load current of the AC microgrid remains almost unchanged (see Figs. 13i and j), and the output current of the AC generator remains relatively constant because of its fixed power set point (see Fig. 13L). In addition, the current of the series DC link, responsible for adjusting the voltage delivered to the AC microgrid, rise slightly when the DC load current steps up (see Fig. 13d). Given the droop slope of the DC microgrid sources, the microgrid voltage reduced as much as 0.97 pu (see Fig. 13h), and the output current of the PV unit converter is escalated proportional to the voltage drop by the MPPT control system (see Fig. 13e). Finally, the power factors of the AC microgrid sources, including the generator and the AC grid, are kept constant as displayed in Figs. 13m and n.

In another section of the above-mentioned scenario, after the obviation of the overload of the DC microgrid, the power conversion set point (Pset) of the parallel controller is raised to 0.2 pu (at time of 2.3 s) to transmit the power from the DC to the AC microgrid. By issuing the command of changing the set points as shown in Fig. 13b, the batteries exit the charging mode (see Fig. 13f), and a major part of the required current is provided to be transferred to the AC microgrid through releasing a part of the current of the solar cells (the current spent on charging batteries). A small portion of the required current is supplied by imposing a 3% drop on the voltage of the DC microgrid (see Fig. 13h) as well as the performance of the MPPT control system (see Fig. 13e). With the release of the capacity of the DC microgrid, the required power of the AC microgrid is provided by the parallel DC link (see Figs. 13c). Additionally, during the changes of the power flow, the drawn current from AC grid is reduced (see Fig. 13k), while the AC voltage amplitude (see Fig. 13i), the AC load current (see Fig. 13j) and the produced current of the synchronous generator remains unchanged, and the power

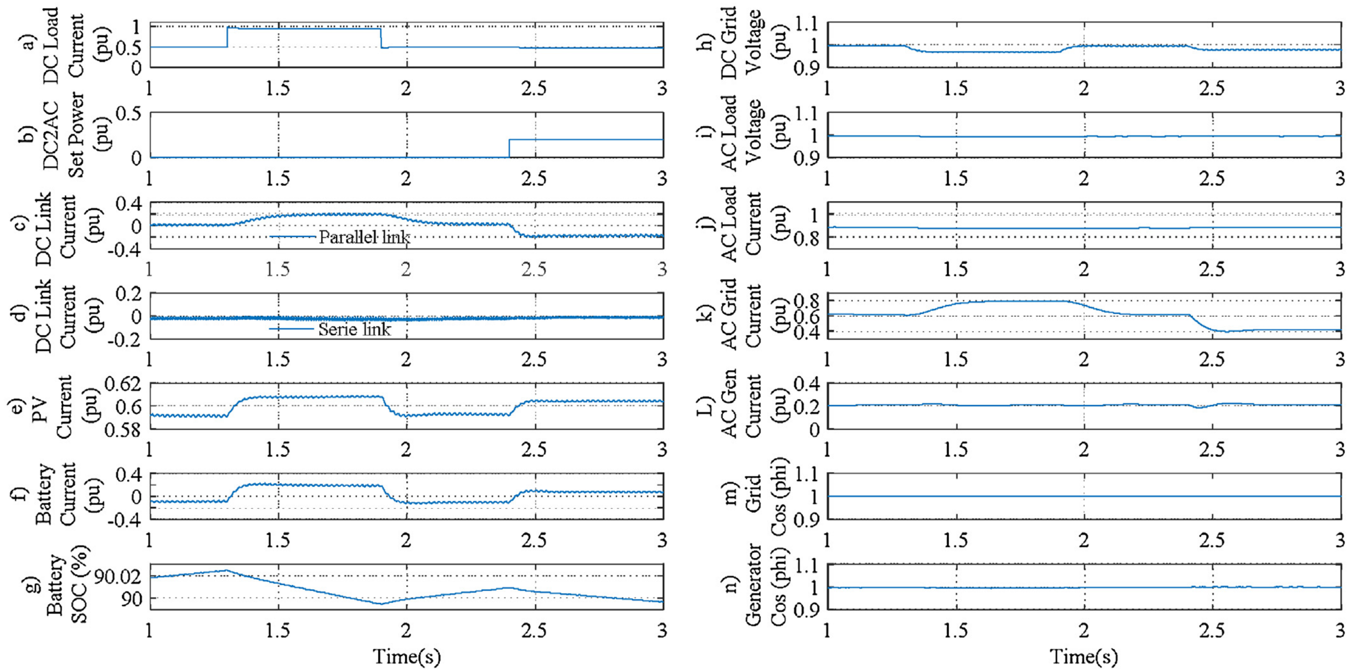

Fig. 13. The overall status of the power flow, voltage control, and power factor correction in the hybrid AC/DC microgrid.

factor of the generator (see Fig. 13n) and AC grid (see Fig. 13m) remains in a unit value.

To evaluate the complete capability of the UPQC-DC controller plan toward controlling the power conversion and power quality of the hybrid AC/DC microgrid simultaneously, the whole voltage and currents of the AC microgrid are analyzed in terms of the total harmonic distortions in the current scenario (see Fig. 14). As can be seen in Fig. 14a, the load current is constant, while the total harmonic distortion is 37%, and the amplitude is 0.87 pu (see Fig. 14a and b). However, the currents drawn from the AC grid (see Fig. 14e and f) as well as the synchronous AC source (see Fig. 14i and j) are almost purely sinusoidal with total harmonic distortions of 2.5%. On the other hand, the voltage of the AC grid is considered strongly harmonic with total harmonic distortions of 70% and an amplitude of 0.93 pu (see Fig. 14c and d). In addition, with appropriate compensation of the series controller, the voltage delivered to the AC load is sinusoidal with total harmonic distortions of 2.5% and an amplitude of 0.99 pu (see Fig. 14g and h). (it is worth noting that all FFTs are applied during 1.5–1.9 s of simulation time in which the maximum currents are exchanged between the two microgrids).

4.2.3. Scenario three

Assumptions

- Connection state: the microgrid is isolated from main grid at second one of simulation.
- Active and reactive loads of AC microgrid: 400 kW and 150 kVar respectively.
- Harmonic contents of AC loads: 150 A of second harmonic, 500 A of fifth harmonic and 200 A of seventh harmonic.
- Available capacity of PV generation: 400 kW.
- Total loads of DC microgrid: 300 kW.
- The AC generator capacity: 300 kW.
- The DC batteries capacity: 100 kWh.

Given the above-mentioned assumptions and the bad conditions of the quality of the load currents as shown in Fig. 15 with 71% of the total harmonic distortions; the voltage and currents of the microgrid in the proposed plan and similar previous plan [20] are compared in Fig. 16. As can be seen, if the traditional hybrid microgrid plan is used, the currents drawn from the AC/DC converter (see Fig. 16c and d) and the synchronous generator (see Fig. 16e and f) will be directly affected by the load current, and the voltage delivered to the load (see Fig. 16a and b) will be inevitably non-sinusoidal. However, unlike all previous articles, it is the first time that the present article employs a series converter instead of employing a parallel one as a synchronous source in the isolated mode, and the possibility of applying a parallel converter, as the power quality compensator, has been provided. Having used the proposed plan in the present study, the currents drawn from the synchronous generator (see Fig. 16k and L) and the series transformer (see Fig. 16i and j) are sinusoidal with total harmonic distortions of 1.5% and 3.75%, and the voltages delivered to the load (see Fig. 16h and g) are almost purely sinusoidal with total harmonic distortions of 2.5%. In the isolated mode, two of the key issues in the microgrids are the power swings and the collapse of the synchronization. As shown in Fig. 16, in the proposed plan, the issue of power swings and exiting the synchronous frequency are completely resolved thanks to a SSVS, and the designed control system did not allow for any microgrid instability (it is worth noting that all FFTs are applied during 2.5–3.0 s of simulation time).

After studying the power quality issues of the voltage and the currents of the hybrid microgrid in the isolated mode, the status of the power conversion, voltage stability and power factor correction in the AC/DC microgrid, are also evaluated. Given the isolated mode, the most important issues facing the microgrid are the power deficit and the voltage drop in addition to the loss of synchronization. In Fig. 17, the most important variables of the hybrid microgrid are shown under the above-mentioned scenario. In the isolated mode, given that the generation capacity of the AC generator was 300 kW and the microgrid load measured 400 kW, the generator of the AC microgrid faced power swings (see Fig. 17j) and drops in voltage (see Fig. 17h) and frequency. As a result, the load current lessened, too (see Fig. 17b). In this regard, given the coordinated AC/DC control system which is sensitive to frequency drops, the parallel DC link injects the required current of the AC microgrid

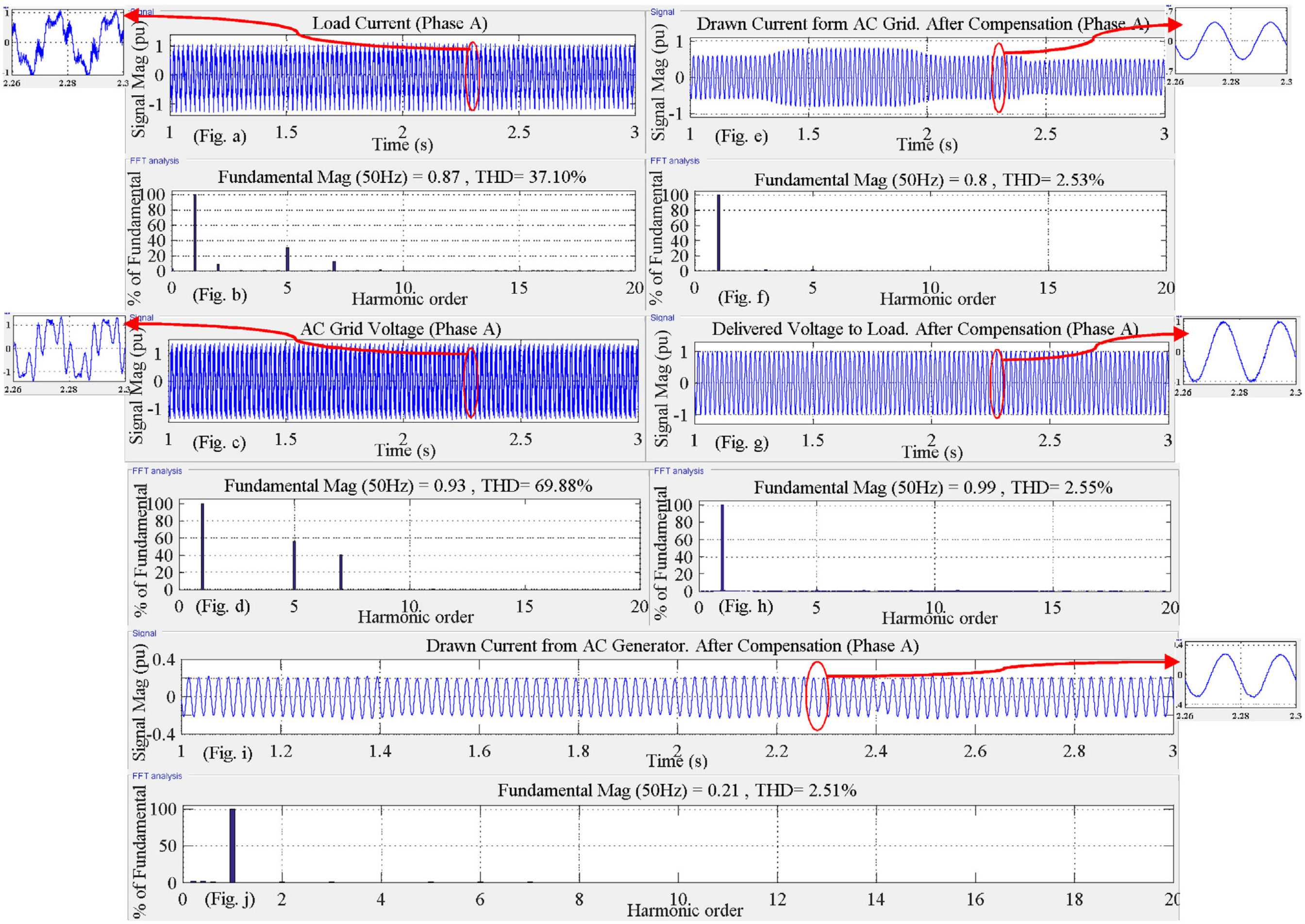

Fig. 14. The whole voltage and currents of the AC microgrid and related harmonic spectrums.

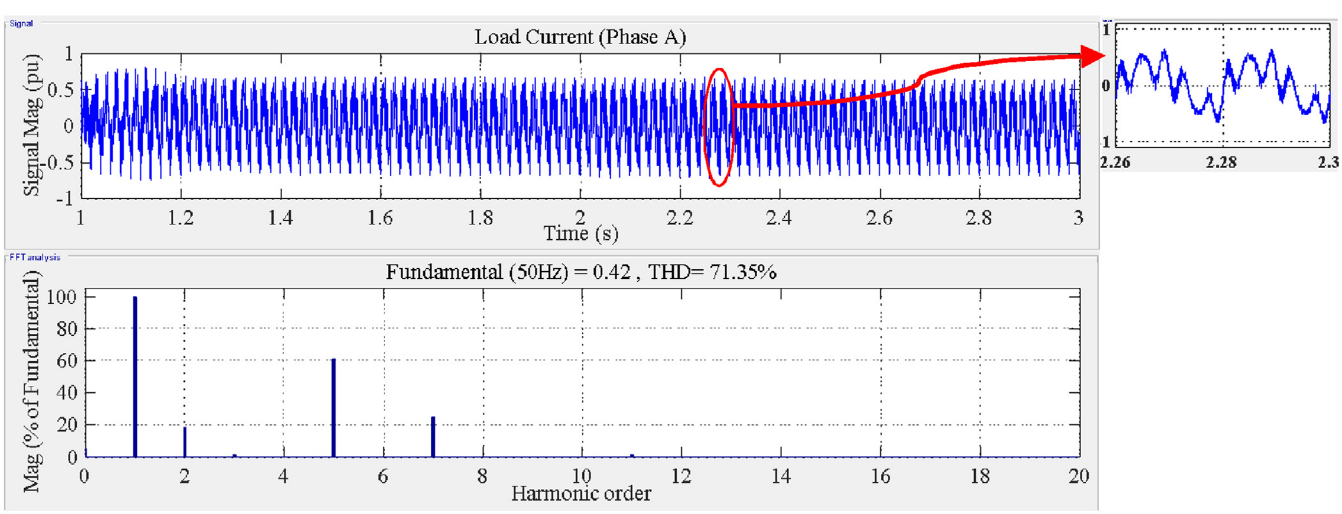

Fig. 15. The load current wave form of phase A and its related harmonic spectrum.

into the system (see Fig. 17c) though imposing the voltage drop on the DC microgrid (see Fig. 17g) during the isolation from the main grid. Moreover, after the stability of the microgrid and transferring the load to the series DC link of the microgrid, the parallel DC link performs its duties, including the full compensation for the reactive power of the load and power quality issues. In the isolated mode, the series DC link is responsible for supplying the energy of the series AC/DC converter with the aim of developing a SSVS, controlling the power swings, and controlling the voltage of the AC microgrid. In this regard, by entering the isolated mode and the occurrence of power swings in the AC generator, the control system of the series AC/DC converter supplies the required current to damp the power swings through the series DC link (see Fig. 17c) and a series transformer (see Fig. 17i). Simultaneous with

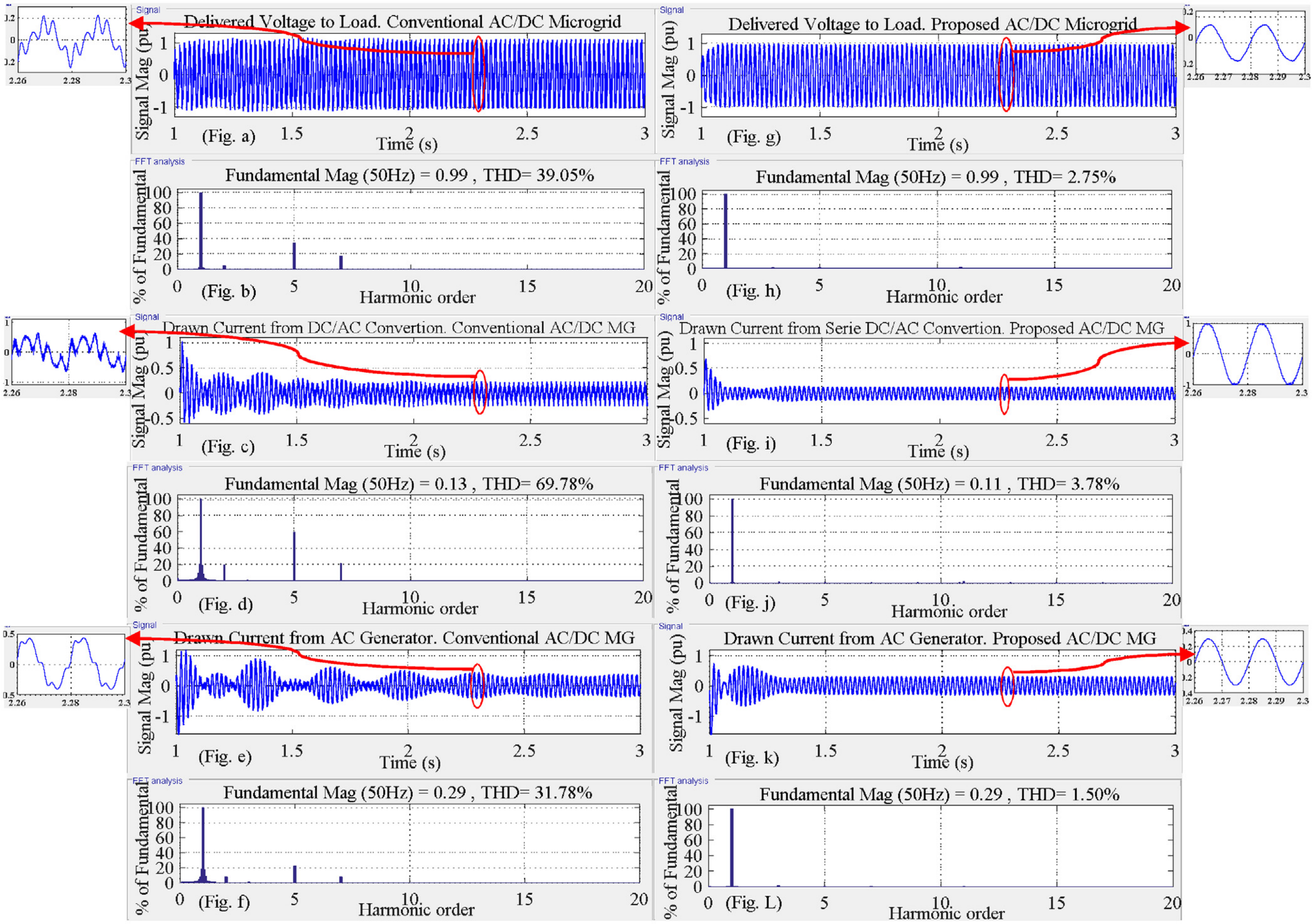

Fig. 16. The voltage and currents of the hybrid AC/DC microgrid in the proposed plan and the conventional plans.

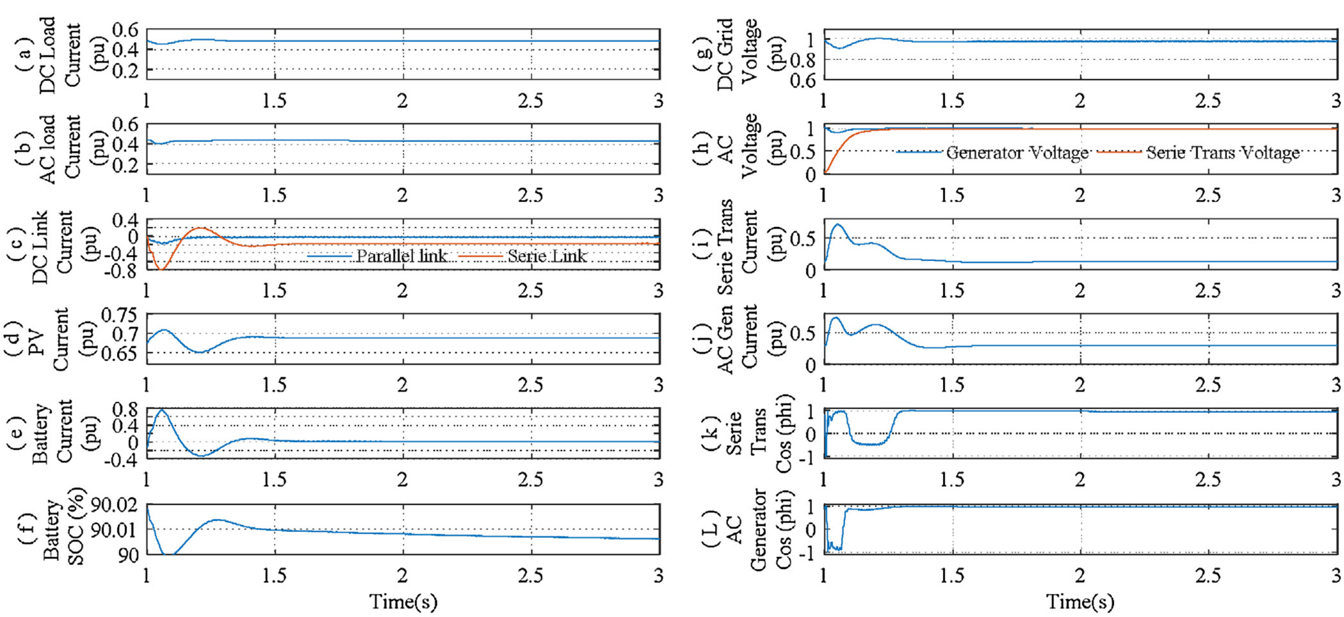

Fig. 17. The overall status of the power flow, voltage control, and power factor correction in the hybrid AC/DC microgrid via isolation from main grid.

controlling the power swings, the series transformer starts making voltage (see Fig. 17h) and after the voltage reaches the nominal value of the microgrid, the series transformer provides the deficit of the current required by the AC microgrid in the form of a static synchronous generator (see Fig. 17i). In this regard, the required current of the series DC link to suppress the power swings is provided through quickly charging and discharging batteries of the DC microgrid (see Fig. 17e and f). The current of the DC microgrid is

Table. 1
The harmonic measurements result for each scenario, including load voltage, grid current and generator current.

Very short time harmonics measurement according to the IEEE Std 519-2014												
Harmonic number	Scenario one			Scenario two			Scenario three			Scenario four		
	Load voltage (%)	AC grid current (%)	Generator current (%)	Load voltage (%)	AC grid current (%)	Generator current (%)	Load voltage (%)	Serie trans current (%)	Generator current (%)	Load voltage (%)	Serie trans current (%)	Generator current (%)
1	100.00	100.00	100.00	100.00	100.00	100.00	100.00	100.00	100.00	100.00	100.00	100.00
2	0.31	0.51	0.51	0.21	0.64	0.81	0.13	0.66	0.26	0.12	0.41	0.29
3	0.62	0.87	1.21	0.72	1.21	1.92	1.24	2.70	0.53	1.14	2.25	0.53
4	0.43	0.27	0.47	0.67	0.33	0.91	0.08	0.37	0.08	0.07	0.34	0.13
5	0.84	0.65	0.74	1.28	1.27	1.46	1.06	2.50	0.35	1.07	1.65	0.40
6	0.52	0.30	0.44	0.67	0.60	0.60	0.09	0.34	0.09	0.08	0.31	0.11
7	0.54	0.82	0.75	0.34	1.15	0.97	0.41	0.92	0.25	0.41	0.86	0.31
8	0.21	0.21	0.20	0.35	0.32	0.31	0.09	0.35	0.09	0.09	0.25	0.09
9	0.50	0.31	0.40	0.47	0.71	0.81	0.28	0.60	0.14	0.32	0.48	0.17
10	0.22	0.18	0.26	0.31	0.27	0.36	0.12	0.33	0.10	0.10	0.25	0.10
11	0.46	0.38	0.34	0.49	0.48	0.49	0.52	0.57	0.25	0.60	0.30	0.26
12	0.26	0.16	0.26	0.25	0.16	0.23	0.09	0.26	0.07	0.10	0.21	0.09
13	0.41	0.17	0.25	0.32	0.32	0.36	0.35	0.35	0.17	0.22	0.31	0.15
14	0.22	0.10	0.17	0.22	0.18	0.24	0.11	0.24	0.08	0.09	0.15	0.07
15	0.42	0.19	0.28	0.37	0.29	0.38	0.23	0.33	0.09	0.23	0.27	0.09
16	0.25	0.10	0.19	0.26	0.20	0.25	0.07	0.20	0.05	0.08	0.13	0.06
17	0.35	0.13	0.18	0.29	0.19	0.26	0.14	0.31	0.08	0.20	0.19	0.10
18	0.25	0.09	0.17	0.20	0.14	0.17	0.10	0.18	0.06	0.12	0.14	0.07
19	0.31	0.10	0.18	0.27	0.17	0.22	0.20	0.18	0.09	0.16	0.16	0.08
20	0.22	0.08	0.17	0.20	0.12	0.14	0.10	0.17	0.06	0.11	0.12	0.07
21	0.36	0.13	0.23	0.28	0.22	0.27	0.20	0.17	0.07	0.19	0.15	0.09
22	0.26	0.09	0.19	0.28	0.19	0.22	0.14	0.14	0.07	0.12	0.11	0.07
23	0.27	0.09	0.18	0.27	0.19	0.22	0.26	0.20	0.10	0.26	0.16	0.10
24	0.21	0.07	0.15	0.19	0.15	0.16	0.16	0.16	0.08	0.19	0.13	0.10
25	0.28	0.07	0.16	0.21	0.13	0.18	0.20	0.17	0.08	0.18	0.15	0.10
26	0.20	0.07	0.16	0.21	0.11	0.15	0.18	0.16	0.08	0.18	0.13	0.09
27	0.25	0.07	0.16	0.24	0.16	0.20	0.28	0.20	0.09	0.21	0.17	0.12
28	0.23	0.09	0.19	0.27	0.15	0.17	0.19	0.13	0.08	0.21	0.12	0.10
29	0.32	0.06	0.17	0.27	0.12	0.16	0.24	0.17	0.10	0.26	0.14	0.11
30	0.23	0.06	0.17	0.27	0.14	0.16	0.19	0.12	0.08	0.29	0.15	0.13
31	0.38	0.06	0.16	0.44	0.15	0.23	0.25	0.14	0.09	0.26	0.11	0.10
32	0.24	0.06	0.17	0.18	0.10	0.11	0.22	0.12	0.09	0.35	0.14	0.14
33	0.31	0.06	0.17	0.28	0.11	0.16	0.40	0.14	0.11	0.44	0.11	0.14
34	0.24	0.06	0.14	0.26	0.16	0.19	0.30	0.13	0.11	0.32	0.10	0.11
35	0.39	0.07	0.21	0.28	0.14	0.17	0.39	0.11	0.11	0.34	0.10	0.13
36	0.27	0.06	0.19	0.24	0.17	0.16	0.28	0.09	0.09	0.36	0.10	0.12
37	0.39	0.06	0.19	0.43	0.20	0.17	0.36	0.12	0.11	0.28	0.08	0.09
38	0.38	0.06	0.18	0.43	0.17	0.19	0.34	0.11	0.10	0.36	0.06	0.10
39	0.40	0.06	0.18	0.57	0.20	0.26	0.34	0.11	0.08	0.43	0.07	0.12
40	0.48	0.08	0.26	0.49	0.20	0.27	0.47	0.10	0.12	0.31	0.04	0.09
41	0.68	0.09	0.31	0.50	0.21	0.24	0.35	0.11	0.09	0.56	0.09	0.14
42	0.52	0.07	0.25	0.62	0.24	0.34	0.39	0.06	0.09	0.32	0.04	0.08
43	0.74	0.08	0.34	0.61	0.20	0.27	0.28	0.12	0.05	0.37	0.06	0.07
44	0.47	0.08	0.29	0.66	0.18	0.31	0.27	0.05	0.06	0.27	0.03	0.05
45	0.56	0.07	0.31	0.36	0.16	0.20	0.35	0.11	0.06	0.27	0.04	0.06
46	0.36	0.07	0.23	0.34	0.14	0.19	0.25	0.05	0.05	0.19	0.03	0.04
47	0.50	0.06	0.28	0.37	0.17	0.23	0.27	0.07	0.05	0.43	0.11	0.06
48	0.39	0.04	0.19	0.30	0.15	0.20	0.29	0.10	0.04	0.23	0.05	0.04
49	0.43	0.07	0.27	0.28	0.17	0.23	0.27	0.15	0.04	0.27	0.07	0.04
50	0.28	0.04	0.19	0.25	0.13	0.17	0.21	0.08	0.03	0.23	0.05	0.03
THD (%)	2.81	1.70	2.33	2.95	2.73	3.42	2.45	4.13	0.97	2.47	3.16	1.06

increased two ways by the voltage drop in the DC microgrid in the isolated mode: firstly, by reducing the load current of the DC microgrid (see Fig. 17a), and secondly, by increasing the current of the boost converter of the PV unit (see Fig. 17d) based on the performance of the MPPT system. Fig. 17k and L display the power factor of the series transformer (SSVS) and the AC generator of the microgrid, respectively. As can be seen, in the event of power swings in the AC generator (during the first 200 ms), the current directions of the series transformer and generator are opposite.

4.2.4. Scenario four

Assumptions

- Connection state: the microgrid is in islanding mode.
- Active and reactive loads of AC microgrid: 400 kW and 150 kVar respectively.
- Harmonic contents of AC loads: 150 A of second harmonic, 500 A of fifth harmonic and 200 A of seventh harmonic.
- Available capacity of PV generation: 500 kW.
- Total loads of DC microgrid: 300 kW.
- The AC generator capacity: 300 kW.
- The DC batteries capacity: 100 kWh.
- DC loads variations: step up the loads to 600 kW during 1.5–2 s.
- AC loads variations: step up the loads to 600 kW and 250 kVar during 2.5–3 s.

Having considered the assumptions as well as the above-mentioned conditions, the variations of the amplitudes of different

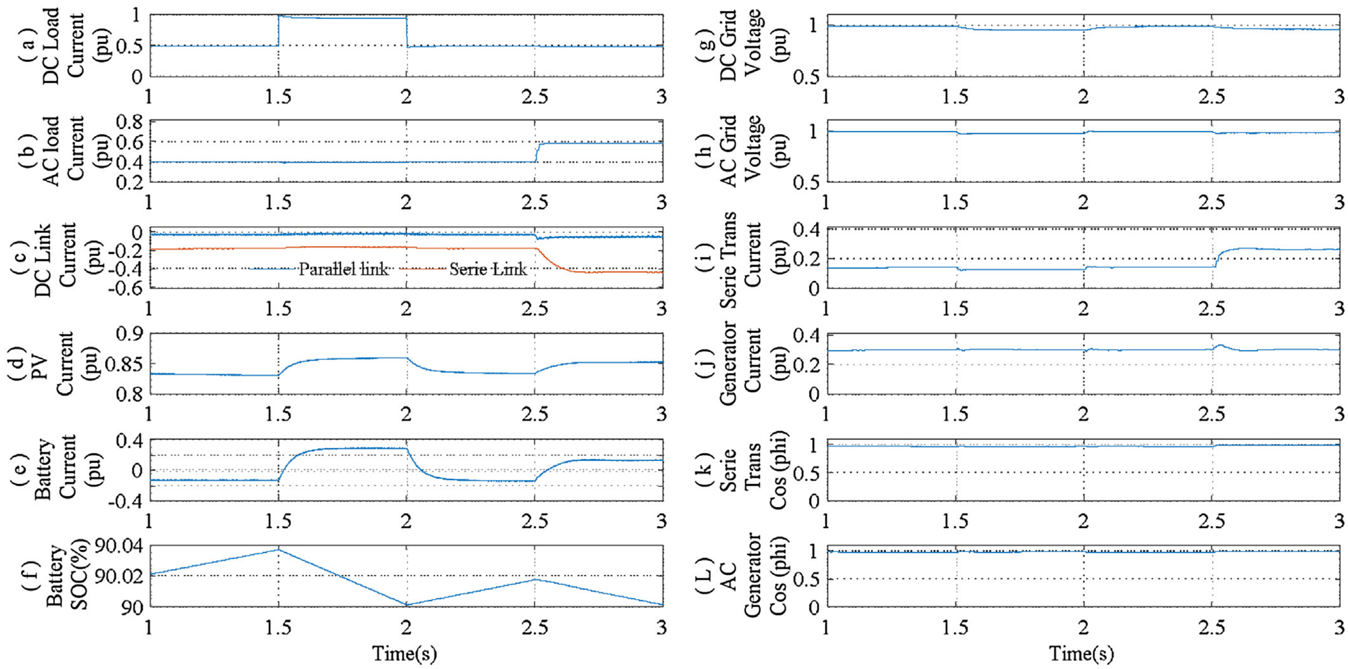

Fig. 18. The overall status of the power flow, voltage control, and power factor correction in the hybrid AC/DC microgrid in the islanding mode.

parameters of AC and DC microgrids are depicted in Fig. 18. Moreover, Fig. 18a displays the changes of the load current in the DC microgrid due to an increase in the load from 300 kW to 600 kW over 1.5–2.0 s. In addition, as can be seen, the load current increased from 0.5 pu to 0.95 pu due to the droop slope of the DC microgrid sources (see Fig. 18g). Given the lack of excess power capacity in the AC microgrid, all of the excess load currents of the DC microgrid are received through the discharge of the batteries of the microgrid (see Fig. 18e) and the maximum power capacity of the solar cells (see Fig. 18d). Given the direct feeding of the SSVS with the voltage of the DC microgrid, the drop of the DC microgrid voltage has some effects on dropping the voltage of the AC microgrid (see Fig. 18h). In addition, the drop of the voltage of the AC microgrid lessens the load current (see Fig. 18b), the series transformer current (see Fig. 18i) and the related DC link current (see Fig. 18c).

Fig. 18b shows the changes of the load current in the AC microgrid due to step up of load from 400 kW to 600 kW over 2.5–3.0 s, and as can be seen, the load current increased from 0.4 pu to 0.57 pu due to the voltage drop of the AC microgrid. Given the 300 kW production limits of the AC microgrid, the deficit of the required power of the AC load should be supplied by the SSVS through the DC link. To this end, with the increase of the load of the AC microgrid from 400 kW to 600 kW, the current of the series DC link (see Fig. 18c) increased from 0.19 to 0.43 pu, and subsequently, the current of the series transformer (see Fig. 18i) experienced a rise from 0.12 to around 0.27 pu. On the other hand, given the increased reactive power of the load from 150 kVar to 250 kVar, the level of the current of the parallel DC link (see Fig. 18c) rise from about 0.03 to 0.05 pu. Given the increased currents of both series and parallel DC links demanded by the AC microgrid, the batteries of the DC microgrid exit charging, whereby the current demanded by the load is provided. In this regard, given the droop characteristics of the DC microgrid, the voltage of the microgrid witnessed about a 3% drop, leading to nearly a 3% increase in the current of the boost converter of the solar power plant. On the other hand, the voltage drops of the DC microgrid caused a small drop in the voltage of the AC microgrid as well. Finally, the power factor of the sources of the AC microgrid are shown in Fig. 18k and L, and as can be seen, these values are constantly kept at a unit value by the proposed control system.

Given the mentioned capability of the proposed plan to realize the objectives of controlling the power flow and maintaining the power quality in the isolated mode simultaneously, the results of the voltage delivered to the load as well as the currents drawn from the sources of the microgrid are depicted in Fig. 19 under the poor quality conditions of the load current and other conditions of this scenario. As can be seen, the voltage delivered to the load as well as the currents drawn from the synchronous generator and series transformers are almost pure sinusoidal (it is worth noting that all FFTs are applied during 2.5–3.0 s of simulation time).

4.3. Harmonic measurements

For the purposes of assessing harmonic levels for comparison with the recommended limits in the IEEE Std 519-2014, harmonic measurements are done for the all mentioned scenarios based on the very short time harmonic measurement method. Very short time harmonic values are assessed over a 3-second interval based on an aggregation of 15 consecutive 10 cycle windows. Individual frequency components are aggregated based on an rms calculation as shown in Eq. (15) where F represents voltage or current, n represents the harmonic order, and i is a simple counter. The subscript vs is used to denote "very short". In all cases, F represents an rms value. The harmonic measurements result is shown in Table 1. Where, for each scenario, three measurements of load voltage, grid current and generator current are done considering harmonic components up to the 50th order. Finally, THD values are calculated based on these harmonic components at the bottom of Table 1. Comparing both individual and total harmonic distortions with recommended harmonic voltage and current limits in Ref. [22], a good aggregation is done in all scenarios.

$$F_{n,vs} = \sqrt{\frac{1}{15}\sum_{i=1}^{15} F_{n,i}\ 2} \tag{15}$$

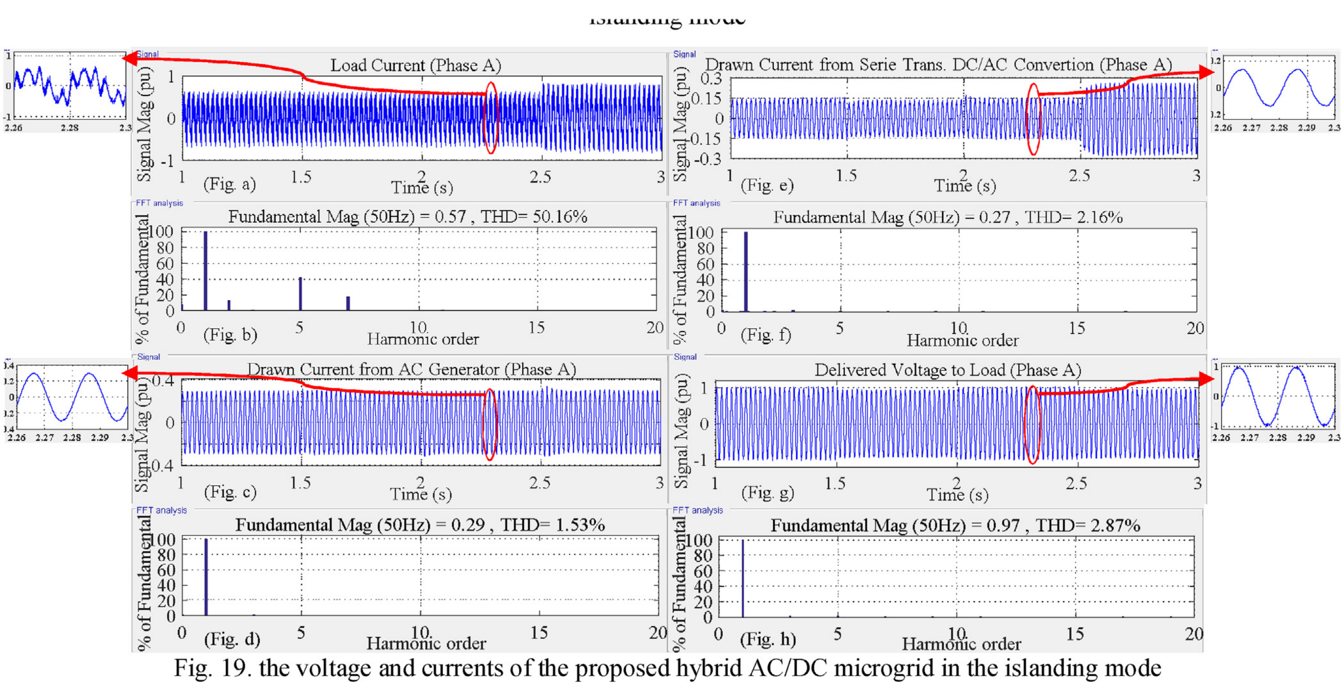

Fig. 19. The voltage and currents of the proposed hybrid AC/DC microgrid in the islanding mode.

5. Conclusion

In this paper, a new unified power quality conditioner named UPQC-DC was introduced and a new proposal was put forward to develop the traditional distribution networks into the hybrid AC/DC smart grids. In this plan, utilizing the capacity of DC microgrid, the possibility of the simultaneous realization of the goals of power quality and power flow control was provided in both the grid connected and isolated modes. According to the proposed functions of the SSVS and APF, the operation of the network in islanded mode is achieved in accordance with the power quality standards even in the worst load quality conditions for the first time. The proposed control system for the series compensator was equipped with a fast response proportional feedback control to damp any power swings and achieve frequency stability. The proposed hybrid control system for the parallel compensator could play the role of the secondary central control for the voltage stability of the DC microgrid. Finally, having investigated the results of four simulated scenarios with poor power quality and the need for spontaneous exchange of power between the AC and DC microgrids, the efficiency of the proposed plan was studied according to the IEEE-519 standards.

Acknowledgment

This paper is supported by Shahid Chamran University of Ahvaz.

Appendix A. Power swing damping

(16) Power swing damping

During the steady state condition, power systems operate on the nominal frequency. The complete synchronism of nominal frequency and voltage at the sending and receiving ends cause complete balance of active and reactive power between generated and consumed powers. Power system faults, line switching, generator disconnection, and the loss or application of large blocks of load result in sudden changes to electrical power. Whereas the mechanical power input to generators remains relatively constant. In this case, the instantaneous mechanical power provided by the turbine is no longer equal to the instantaneous electrical power delivered or required by the load and this will cause oscillations in rotor angle and can result in severe power swings. the strategy for power swing control is developed based on the transient energy function. The approach adopted to develop the series compensator control strategy relies on the fact that to damp the low frequency oscillations (power swings), the energy function must reduce with time. This requires the time derivative of the energy function of the system with the series voltage controller to be less than or equal to zero. The control law has been developed for a single machine infinite bus system under the assumption that the generator dynamics are represented by a classical model. With usual notations, the energy function for a lossless single machine infinite bus system with synchronous generator is given by the expression.

$$E = \frac{1}{2}M\omega^2 - \frac{E_g E_b}{X}(\cos\delta - \cos\delta_0) - P_m(\delta - \delta_0) \tag{16}$$

In the above equation δ_0 is the rotor angle at the stable operating point. The time derivative of Eq. (16) is given by

$$\frac{dE}{dt} = \left(M\frac{d\omega}{dt} - P_m\right)\frac{d\delta}{dt} + \frac{E_g E_b \sin\delta}{X}\frac{d\delta}{dt} = -P_e\frac{d\delta}{dt} + \frac{E_g E_b \sin\delta}{X}\frac{d\delta}{dt} \tag{17}$$

The insertion of a voltage source Ep in the system is equivalent to connecting a series resistance Rs in the line. The generated power P_e with the series controller is given by

$$P_e = \frac{R_s E_g^2 - R_s E_g E_b \cos\delta + E_g E_b X \sin\delta}{R_s^2 + X^2} \tag{18}$$

substituting Eq. (18) in Eq. (17), the expression for the rate of change of energy with time is obtained as

$$\frac{dE}{dt} = -\frac{R_s(1 - \cos\delta)\omega}{X^2} \tag{19}$$

Note: In deriving Eq. (18) it is assumed that ${R_s}^2 \ll X^2$ and $E_g = E_b = 1$ pu.

Table A1
Specification of the model distribution system of Fig. 8.

Medium voltage network		Distribution transformer		Arc furnance transformer	
Nominal voltage	20 kV	Nominal power	2 MVA	Nominal power	5 MVA
Frequency	50 Hz	Nominal rate	20/0.4 kV	Nominal rate	20/0.7 kV
Source resistance	5 Ω	Frequency	50 Hz	Frequency	50 Hz
Source reactance	2 Ω	Winding connection	Yyn	Winding connection	Yyn
Ground resistance	10 Ω	R1	0.001 pu	R1	0.005 pu
Distribution lines		L1	0.05 pu	L1	0.05 pu
ZL1	0.01 + j0.003 Ω	R2	0.001 pu	R2	0.005 pu
ZL2	0.03 + j0.006 Ω	L2	0.05 pu	L2	0.05 pu
ZL3	0.1 + j0.3 Ω	Nonlinear load			
ZL4	0.01 + j0.08 Ω	Thyristor-controlled rectifier		Firing angle $\alpha = 0$	$I_{DC} = 700$ A
Unbalanced linear load		Critical loads			
Za	0.08 + j0.06 Ω	Three phase thyristor-controlled rectifier		Firing angle $\alpha = 30$	$I_{DC} = 10$ A
Zb	1 + j0.7 Ω	Single phase thyristor-controlled rectifier		Firing angle $\alpha = 45$	$I_{DC} = 10$ A
Zc	0.03 + j0.006 Ω	Single phase diode rectifier			$I_{DC} = 5$ A

Table A2
Specification of the model hybrid AC/DC microgrid of Fig. 10.

AC generator		AC grid		AC transformer	
Nominal power	300 KVA	Nominal power	15 MVA	Nominal power	1 MVA
L-L voltage	400 V	L-L voltage	20 kV	Nominal rate	20/0.4 kV
Frequency	50 Hz	Frequency	50 Hz	Frequency	50 Hz
Rs (stator resistance)	0.007 pu	First harmonic	1.00 pu	Winding connection	D1yn
Ll (stator leakage inductance)	0.19 pu	Fifth harmonic	0.55 pu	R1	0.002 pu
Lmd (d-axis magnetizing inductance)	1.51 pu	Seventh harmonic	0.40 pu	L1	0.08 pu
Lmq (q-axis magnetizing inductance)	1.46 pu	HV line impedance	5 + j2 Ω	R2	0.002 pu
Rf (field resistance)	0.0011 pu	LV lines impedance	0.5 + j0.1 Ω	L2	0.08 pu
Llfd (field leakage inductance)	0.12 pu	PV on DC grid		Rm	500 pu
Rkd (d-axis damper resistance)	0.014 pu	Nominal power	500 kW	Lm	500 pu
Llkd (d-axis damper leakage inductance)	0.081 pu	Nominal voltage	600 V	Parallel AC/DC controller	
Rkq1 (q-axis damper resistance)	0.001 pu	PV MPPT converter		K_{DC}	0.09 V/kW
Llkq1 (q-axis damper leakage inductance)	0.81 pu	MPPT PWM freq	5000 Hz	K_{AC}	0.077 (rad/s)/kW
Rkq2 (q-axis damper resistance)	0.009 pu	Time window MPPT	0.0002 s	Kw	20 kW/(rad/s)
Llkq2 (q-axis damper leakage inductance)	0.089 pu	Rdc	0.002 A/V	DC link capacitance	5000 μF
Turbine, governor & exciter		Filter inductance	1 mH	Filter inductance	0.4 mH
T_G (governer time constant)	0.02 s	Filter capacitance	3000 μF	Hysteresis frequency	10 kHz
T_{trb} (turbine time constant)	0.01 s	Battery on DC grid		Serie AC/DC controler	
K_{fd} (exciter gain)	0.07	Nominal power	100 kWh	Kw	20 kW/(rad/s)
T_{fd} (exciter time constant)	0.08 s	Nominal voltage	600 V	Filter inductance	0.3 mH
H (rotor inertia)	0.2 s	Rbat	0.05 ohm	Filter capacitance	22 μF
		Converter drop coefficient	0.0025 A/V	PWM frequency	6 kHz

For $\frac{dE}{dt} \leq 0$ the sufficient condition is

$$R_s \propto (1 - \cos \delta)\omega \tag{20}$$

Introducing a proportionality constant K where $K > 0$

$$R_s = K(1 - \cos \delta)\omega \tag{21}$$

Since $E_p = I_m R_s$ the expression for the real voltage E_p is given by

$$E_p = K I_m (1 - \cos \delta)\omega \tag{22}$$

Linearizing the Eq. (22) (and since $\omega_0 = 0$), the control law for series voltage control is obtained as

$$\Delta E_p = K_\omega \Delta\omega \tag{23}$$

References

[1] J.J. Justo, F. Mwasilu, J. Lee, J. Jung, AC-microgrids versus DC-microgrids with distributed energy resources: a review, Renew. Sustainable Energy Rev. 24 (2013) 387–405.
[2] A.T. Elsayed, A.A. Mohamed, O.A. Mohammed, DC microgrids and distribution systems: an overview, Electr. Power Syst. Res. 119 (2015) 407–417.
[3] H. Lotfi, A. Khodaei, AC versus DC microgrid planning, IEEE Trans. Smart Grid 8 (2017) 296–304.
[4] R. Majumder, Aggregation of microgrids with DC system, Electr. Power Syst. Res. 108 (2014) 134–143.
[5] N. Eghtedarpour, E. Farjah, Power control and management in a hybrid AC/DC microgrid, IEEE Trans. Smart Grid 5 (2014) 1494–1505.
[6] C.N. Papadimitriou, E.I. Zountouridou, N.D. Hatziargyriou, Review of hierarchical control in DC microgrids, Electr. Power Syst. Res. 122 (2015) 159–167.
[7] T.V. Vu, D. Perkins, F. Diaz, D. Gonsoulin, C.S. Edrington, T. El-Mezyani, Robust adaptive droop control for DC microgrids, Electr. Power Syst. Res. 146 (2017) 95–106.
[8] A. Radwan, Y.A.R. Mohamed, Networked control and power management of AC/DC hybrid microgrids, IEEE Syst. J. 99 (2014) 1–12.
[9] F. Nejabatkhah, Y.W. Li, Overview of power management strategies of hybrid AC/DC microgrid, IEEE Trans. Power Electr. 30 (2015) 7072–7089.
[10] M. Hosseinzadeh, F. Rajaei Salmasi, Power management of an isolated hybrid AC/DC micro-grid with fuzzy control of battery banks, IET Renew. Power Gen. 9 (2015) 484–493.
[11] R. Majumder, A hybrid microgrid with DC connection at back to back converters, IEEE Trans. Smart Grid 5 (2014) 251–259.
[12] H. Xiao, A. Luo, Z. Shuai, G. Jin, Y. Huang, An improved control method for multiple bidirectional power converters in hybrid AC/DC microgrid, IEEE Trans. Smart Grid 7 (2016) 340–347.
[13] P. Wang, C. Jin, D. Zhu, Y. Tang, P.C. Loh, F.H. Choo, Distributed control for autonomous operation of a three-port AC/DC/DS hybrid microgrid, IEEE Trans. Ind. Electron. 62 (2015) 1279–1290.
[14] A.A. Abdelsalam, H.A. Gabbar, A.M. Sharaf, Performance enhancement of hybrid AC/DC microgrid based D-FACTS, Int. J. Electr. Power 63 (2014) 382–393.
[15] C. Wang, X. Yang, Z. Wu, Y. Che, L. Guo, S. Zhang, Y. Liu, A highly integrated and reconfigurable microgrid testbed with hybrid distributed energy sources, IEEE Trans. Smart Grid 7 (2016) 451–459.
[16] J.M. Guerrero, M. Chandorkar, T.L. Lee, P.C. Loh, Advanced control architectures for intelligent microgrids—part II: power quality, energy storage, and AC/DC microgrids, IEEE Trans. Ind. Electron. 60 (2013) 1263–1270.
[17] S.A. González, M.I. Valla, UPQC implemented with cascade asymmetric multilevel converters, Electr. Power Syst. Res. 124 (2015) 144–151.
[18] T. Lv, Q. Ai, Y. Zhao, A bi-level multi-objective optimal operation of grid-connected microgrids, Electr. Power Syst. Res. 131 (2016) 60–70.

[19] Z. Zeng, H. Yang, R. Zhao, C. Cheng, Topologies and control strategies of multi-functional grid-connected inverters for power quality enhancement: a comprehensive review, Renew. Sustainable Energy Rev. 24 (2013) 223–270.
[20] B. Han, B. Bae, H. Kim, S. Baek, Combined operation of unified power-quality conditioner with distributed generation, IEEE Trans. Power Deliv. 21 (2006) 330–338.
[21] V. Khadkikar, Enhancing electric power quality using UPQC: a comprehensive overview, IEEE Trans. Power Electron. 27 (2012) 2284–2297.
[22] IEEE Std 519-2014, IEEE recommended practices and requirements for harmonic control in electrical power systems, 2015.
[23] IEEE Std 1159-1995, IEEE recommended practice for monitoring electric power quality, 1995.
[24] N. Yang, B. Nahid-Mobarakeh, F. Gao, D. Paire, A. Miraoui, W. Liu, Modeling and stability analysis of multi-time scale DC microgrid, Electr. Power Syst. Res. 140 (2016) 906–916.
[25] R.J. Hamidi, H. Livani, S.H. Hosseinian, G.B. Gharehpetian, Distributed cooperative control system for smart microgrids, Electr. Power Syst. Res. 130 (2016) 241–250.
[26] M. Mehrasa, E. Pouresmaeil, B.N. Jørgensen, J.P.S. Catalão, A control plan for the stable operation of microgrids during grid-connected and islanded modes, Electr. Power Syst. Res. 129 (2015) 10–22.
[27] M. Marzband, M.M. Moghaddam, M.F. Akorede, G. Khomeyrani, Adaptive load shedding scheme for frequency stability enhancement in microgrids, Electr. Power Syst. Res. 140 (2016) 78–86.
[28] E. Fuchs, M.A.S. Masoum, Power Quality in Power Systems and Electrical Machines, second ed., Elsevier, 2015.
[29] H. Akagi, E. Hirokazu, M. Aredes, Instantaneous Power Theory and Applications to Power Conditioning, first ed., Wiley, 2007.